Chapter 1

Biomimetic and Electrodeposited Calcium-Phosphates Coatings on Ti – Formation, Surface Characterization, Biological Response

Marcin Pisarek, Agata Roguska, Lionel Marcon and Mariusz Andrzejczuk

Additional information is available at the end of the chapter

http://dx.doi.org/10.5772/48693

1. Introduction

Engineering of materials (metals and their alloys) with a controlled and surface morphology in nanoscale is important due to their potential applications in biomedicine and catalysis. Titanium dioxide (TiO_2) has attracted the attention of scientists and engineers for its unique properties and has also been considered in above mentioned applications [1]. TiO_2 nanostructures offer encouraging implications for the development and optimization of novel substrates for biological research [2,3] and spectroscopic (SERS: Surface Enhanced Raman Spectroscopy) investigations: absorbate-adsorbate systems [4-6]. Titanium oxide layers with controlled morphology have been reported to stimulate apatite formation in the living environment in vitro or simulated body fluid to a greater extent than smooth native oxide layers on titanium [7]. In addition, TiO_2 nanostructures can act as an anchor of ceramic top coating and improve mechanical interlocking between the coating and the substrate [2]. However, only a few studies have reported modifications to the surface roughness as well as the chemistry at the nanometer scale in a reproducible and cost effective manner [8-11].

In recent years, there has been increasing interest in the formation of porous bioactive surface layers on titanium substrates, which would contribute to an increase of the surface roughness and the specific surface area provided for the subsequent coating deposition via biomimetic methods (prolonged soaking in simulated body fluid, e.g. Hanks'solution, under physiological conditions) [7,12-14]. Since the heterogeneous nucleation ability of calcium and phosphate ions is directly dependent on a proper "activation" of metal surface, different Ti pretreatments such as alkali treatment [14-18], acid treatment [7,9,10,14], H_2O_2 treatment [11,19], and anodic oxidation treatment in a solution containing fluoride ions have been investigated to form bioactive porous oxide layers on Ti [2,3,20-22]. The purpose of those

pretreatments is mainly to modify the surface topography, the chemical composition and structure of the oxide layer, and to form a new surface layer. Electrochemical processes are also commonly applied for modifying surfaces of Ti to increase its biocompatibility through direct electrodeposition from Hanks' solution [23,24]. The resulting chemical composition is close to that of hydroxyapatite, one of the few materials that support bone ingrowth and osseointegration when used in orthopedic or dental applications [25,26]. Both biomimetically and electrochemically deposited calcium phosphate coatings are considered as promising alternatives to conventional plasma spraying hydroxyapatite [25,27].

The nucleation and growth of calcium phosphates on titanium oxides has been extensively investigated because of their relevance to orthopedic applications. It is well known that Ca-P coatings have led to better clinical success rates in long term than uncoated titanium implants. These advantages are due to superior initial rate of osseointegration. The apatite coatings deposited on different biomaterials (metals and their alloys, polymers) can reduce fibrous encapsulation, promote bone growth, enhance direct bone contact and has also been shown to promote differentiation of bone marrow stromal cells along osteogenic lineage [28]. The design of novel Ca-P coatings involves also addition of small amount of metal or metal oxides nanoparticles exhibiting antibacterial activity. Such nanoparticle incorporated to Ca-P coatings may impart antibacterial property, which makes them promising to be applied in hard tissue replacement against postoperative infections. However, it is worth to mention, that the size and amount of such nanoparticles should be properly chosen, in order to prevent their toxic effect to living cells [29].

In this chapter a two-step procedure, based on chemical and electrochemical methods aimed at activating titanium surface for subsequent deposition of calcium phosphate coatings, is presented. The combined effects of surface topography and chemistry of Ti substrate on calcium phosphate formation are discussed. The calcium phosphate coatings produced by both biomimetic as well as electrochemical methods are compared with respect to their physicochemical characteristics and biological evaluation.

2. Body (problem statement, application area, research course, method used, status, results, further research)

To date, studies of modified Ti surfaces for biomedical purposes have focused on characterization of their morphology and physicochemical properties. Interest in those properties stems from the fact that such materials display high corrosion resistance through a wide pH range as well as in solutions containing aggressive ions in comparison with metallic materials not based on Ti. Data in the literature indicate that many centers in the world try to highlight the chemical composition of oxide layers based on titanium: on defining the chemical state of the elements of which such layers are composed, and defining varieties of the polymorphic forms of titanium dioxide which constitutes the main component of such layers (structural research) [19,30].

The basic factors characterizing a material's surface and significantly affecting the biological processes occurring at the material-cell/tissue interface include its surface topography, chemical and phase composition, and physicochemical properties (e.g. wettability). In spite of intensive studies worldwide, no definitive criteria have yet been established to describe the optimal topographical/morphological features of a biomaterial in relation to particular cell lines. It is known, however, that titanium oxides materials having a relatively highly developed surface should show improved integration with bone tissue. It has also been observed that a titanium surface having a well-developed morphology and high porosity accelerates collagen synthesis and supports bone mineralization. The application of appropriate methods of modifying the surface of the biomaterial has a significant impact on adhesion and the rate of cell growth [31,32]. It must be considered, however, that the cells present at the tissue/material interface will react differently to the particular properties of the implant surface. Contact between the biomaterial and cells, tissues and body fluids results in extra-cellular matrix proteins being spontaneously deposited on the surface, forming a biofilm. Cells adhere through integrin receptors and a specific arrangement of extra-cellular matrix proteins. The resulting complex determines cell behavior including their ability to proliferate and migrate. The distribution and thickness of the biofilm depends on the surface properties of the biomaterial, and mainly on its chemical composition and morphology [33].

Chemical processes for modifying surfaces of Ti and its alloys are widely employed to increase the biocompatibility of those materials. Such methods as Ti etching in alkaline solutions (e.g. NaOH [9,14-18,30,32,34]), acidic solutions (e.g. H_2SO_4, H_3PO_4 [9,14,32]) or hydrogen peroxide (H_2O_2 [11,19]) at high temperatures, combined with subsequent prolonged soaking of samples in artificial physiological solutions (SBF- Simulated Body Fluid, Hanks solution) at pH~7, make it possible to obtain porous oxide layers with built-in ions of calcium and phosphorous [12,14,16,18,22,35]. The chemical composition of the coatings obtained in this way is close to that of hydroxyapatite, one of the most effective materials for increasing biocompatibility. The anodic oxidation of Ti and its alloys in acidic or neutral solutions containing fluorides is a typical electrochemical method for obtaining oxidized layers of different thicknesses, uniform chemical composition and refined nanoporosity [2,3,5,20-22,36]. The addition of an electrolyte of suitable fluoride concentration can ensure that a porous morphology is obtained, in the form of 'honeycomb' titanium oxide nanotubes[20-22]. Such structures can provide very promising substrates which increase biological tolerance, because they allow to precisely control the thickness of layers (by the end voltage of the anodic polarization) and surface morphology (porosity). Further chemical treatment is made to introduce other factors increasing biotolerance, in the form of ions of calcium and phosphorus, by immersing the oxide layers in artificial physiological solutions [22,37-40] or by electro-deposition from the same solutions [41,43]. Such surface modification of titanium may play an additional role providing protection against the action of the biological environment and thus restricting the penetration of metal ions into the organism. This is particularly important because of the increasing frequency of titanium allergies, even though titanium was long considered biologically inert.

One unfortunate phenomenon associated with implant surgery is the high risk of post-operative infections. The adherence of bacteria to the biomaterial causes surgical complications, and poses a particularly serious threat to patients with long-term implants. It is true that modern, effective methods of sterilization now exist which reduce the risk of complications from infection, yet in the case of the early onset of corrosion of the implant, problems with bacterial habitats do arise [43,44]. Post-operative infections can be counteracted by silver nanoparticles on the surface of the biomaterial, since their antibacterial properties are well demonstrated [45,46]. The bactericidal properties of silver nanoparticles largely result from the size of the particles, which allows such structures to penetrate easily through biological membranes to the interior of microorganisms. At the same time, studies indicate that silver has no toxic effect on human cells (limphocytes, fibroblasts and osteoblasts) [29] if the concentration of silver ions in the body fluids is below 10 mg/l [47].

The following materials and methods were used for preparation and characterization of biomimetic coatings:

- Material substrate: 0.25 mm-thick Ti foil (99.5% purity, Alfa Aesar, USA), all samples before any treatment were ultrasonically cleaned with deionized (DI) water, rinsed with acetone and ethanol and dried in air.
- Chemical pretreatment: the samples were soaked in a 3 M NaOH aqueous solution at 70^{o}C for 24 h, or in an H_3PO_4 + H_2O_2 mixture (with a volume ratio of 1:1) at room temperature for 24 h.
- Electrochemical pretreatment: titanium oxide nanotube layers were fabricated by anodic oxidation of Ti in an optimized electrolyte of NH_4F (0.86 wt.%) + DI water (47.14 wt.%) + glycerol (52 wt.%) at room temperature, applied voltage V_{max} from 10 V up to 25 V. After anodization, the samples were annealed in air at 600^{o}C for 1 or 2 h.
- The annealed nanotubes were covered with a thin Ag layer by the sputter deposition technique in a vacuum (p = 3 x 10^{-3} Pa), using a JEE-4X JEOL device, in a configuration perpendicular to the surface of the samples. Ag of spectral purity was used. The average amount of the metal deposited per cm^2 was estimated from the mass gain of the samples. Both the true average and local amount of the metal deposits may actually vary substantially due to the highly-developed specific surface area of the TiO_2 nanotube/Ti substrate.
- Mechanical properties: nano-hardhness, Young's modulus, of anodic oxide layers and Ca-P coatings on a Ti before and after heat treatment were measured using the Hysitron Nanoindenter device equipped with a Berkowich intender. The indentation parameters were as follows: a loading rate of 0.1 mN/s to a maximum load of 1 mN for period of constant load of 2 s. From the measurements, nano-hardness, H, and reduced Young's modulus, Er, were determined according to the standard procedures [48]. Average values were calculated from 8 to 12 measurements for each sample.
- Deposition of biomimetic calcium phosphate coatings on Ti oxide or Ti substrate. The samples were exposed to a stagnant Hanks' solution in a plastic vessel and kept in a glass thermostat at 37^{o}C for 6 h up to 7 days. All samples were washed with distilled water and eventually dried in air at 250^{o}C for 1 h. The direct electrodeposition of

calcium phosphates was performed at laboratory temperature for 2h 15 min in a conventional cell fitted with an Ag/AgCl (3 M KCl) electrode maintaining the cathodic potential of – 1.5 V vs OCP potential (10 min). Titanium substrates were used as cathodes for electrodeposition. The cathodic polarization process was performed using an AutoLab PGSTAT 302N (Ecochemie) potentiostat/galvanostat.

- The Hanks' solution was prepared by dissolving reagent-grade (g/L): NaCl 8.00, KCl 0.40, $Na_2HPO_4 \cdot 2H_2O$ 0.06, KH_2PO_4 0.06, $MgSO_4 \cdot 7H_2O$ 0.20, $NaHCO_3$ 0.35, $CaCl_2$ 0.14 into distilled water and buffering at pH = 7.4.
- For the morphological characterization of the samples top-view and cross-sectional examinations were carried out with a high resolution scanning electron microscope (Hitachi S-5500). A Thermo Noran spectrometer coupled with a Hitachi S-5500 scanning electron microscope was used for local EDS analysis.
- The surface topography of the chemically treated samples was examined by AFM (MultiMode V, Veeco). AFM images were recorded in contact mode using silicon cantilevers with a resonance frequency of 250–300 kHz. The investigated surfaces were scanned within the area of 1 μm^2. The estimation of the surface roughness parameters, the average roughness (Ra), root-mean-square deviation (R_q), the mean roughness depth (Rz) and maximum roughness depth R_{max}, was done using the Nanoscope 7.2 software (Veeco).
- A single focused ion beam (FIB) Hitachi FB-2100 system (Hitachi High Technologies Corporation, Japan) was used for TEM specimen preparation. A gallium source ion beam with applied accelerating voltage 40 kV during FIB milling, and 10 kV for final thinning, was used. This system allowed for lift-out sample preparation technique to be used in order to obtain a thin TEM lamella. The thickness of the lamella, as measured by cross-section observations in FIB, was less than 100 nm. The samples prepared by FIB milling were examined with a high resolution scanning transmission electron microscope (Hitachi HD- 2700, Hitachi High-Technology Co., Tokyo) operating at an accelerating voltage of 200 kV and with transmission electron microscope (TEM Jeol 1200) operating at an accelerating voltage 120V.
- The chemical composition of the surface of the samples, with and without the calcium phosphate coatings and after adsorption of the proteins, was characterized by Auger electron spectroscopy and X-ray photoelectron spectroscopy (Microlab 350). For XPS used $Al_{K\alpha}$ non-monochromated radiation (1486.6 eV; 300 W) as the exciting source. The pressure during the analysis was 5.0×10^{-9} mbar. The binding energy of the target elements (Ti 2p, O 1s, C 1s, Ca 2p, P 2p, Cl 2p, Mg 1s, Na 1s, N1s) was determined at a pass energy of 40 eV, with a resolution of 0.83 eV, using the binding energy of carbon (C 1s: 285 eV) as the reference. A linear or Shirley background subtraction was applied to obtain XPS signal intensity. The peaks were fitted using an asymmetric Gaussian/Lorentzian mixed function. Fourier transform infrared spectroscopy (FT-IR; Nicolet 6700, Thermo Electron Corporation) was used to analyze the phase composition of the calcium phosphate coatings after incubation in Hanks' solution and adsorption of the proteins. Measurements were made using the attenuated total reflectance (ATR) technique. Each sample was scanned 64 times at a resolution of 4 cm^{-1} over a frequency range of 400–4000 cm^{-1}.

- The crystal structure of the substrate materials was determined from the XRD patterns using a Philips PW 1830 X-ray diffractometer equipped with a Cu source (Kα line 0.1541837 nm) and X-Pert goniometer. The accelerating voltage was 40 kV, the current 30 mA, and the range of scattering angle 2θ - from 35 up to 100 deg.
- Protein adsorption. Bovine serum albumin (BSA) (Sigma, purity of 99.8%) was used as a model protein in this study. Phosphate buffered saline (PBS, pH = 7.4) was used to prepare the protein solution (10 mg protein / 1 ml PBS), 100 μl of which were pipetted onto the samples' surface coating in a cell culture plate. The plate was then placed in an incubator at 37°C for 20 min. All the samples (before and after immersion in Hanks' solution) were examined immediately after termination of the preparation procedure.
- Living cells attachment. Human osteosarcoma U2OS cells were used to evaluate the biocompatibility of the Ca-P coatings under study. Dulbecco's modified eagle's medium (DMEM, Invitrogen) supplemented with 10% fetal bovine serum (Invitrogen) and 1% of a penicillin/streptomycin mixture was used as a cell culture medium. Cells were seeded on the sample surfaces at 1.0×10^4 cells/cm^2 and cultured at 37°C in a humidified atmosphere containing CO_2 for 24, 48, 72 and 120 h. Afterwards, double fluorescent labeling of the cell nuclei and membranes was performed. The cell nuclei were stained with Hoechst 33342 (Invitrogen), and the cell membranes were stained with Vybrant DiI (Molecular Probes) according to the manufacturers' instructions. Morphology of the cells was examined using a fluorescence microscope (Eclipse 80i, Nikon Instruments, Tempe, AZ). All samples were sterilized by autoclaving at 121°C for 20 min prior to the cell culture experiments [49,50].
- The silver ion release from Ag/TiO_2 nanotube/Ti samples was measured by inductively coupled plasma mass spectrometry (ICP-MS, Elan 9000 Perkin Elmer). The samples were incubated in 10 ml of deionized water or 0.9% NaCl solution at room temperature without stirring. The amounts of released silver were determined by analyzing the resulting solution.

- **Titanium oxides as potential substrates for deposition of Ca-P coatings: fabrication methods and physicochemical characteristics**
  - **a. Formation of nanoporous TiO_2 layers on Ti by chemical etching or electrochemical methods**
  - **b. Surface and structure characterization**
  - **c. Surface roughness and wettability**

The biocompatibility of titanium as an implant material is attributed to the surface oxides spontaneously formed in air [51,52] and/or physiological fluids [33]. It is known that the protective and stable oxides on titanium are favorable for osseointegration [53]. Stability of the oxide depends strongly on its composition, structure and thickness. Among various methods aimed at improving the interfacial properties and lifetime of Ti-based implants [54], anodization and chemical etching methods have attracted considerable attention because of their simplicity and their controllable, reproducible results [7,55].

Fig. 1 shows SEM images of surface morphology of Ti foil (0.25 mm in thickness).

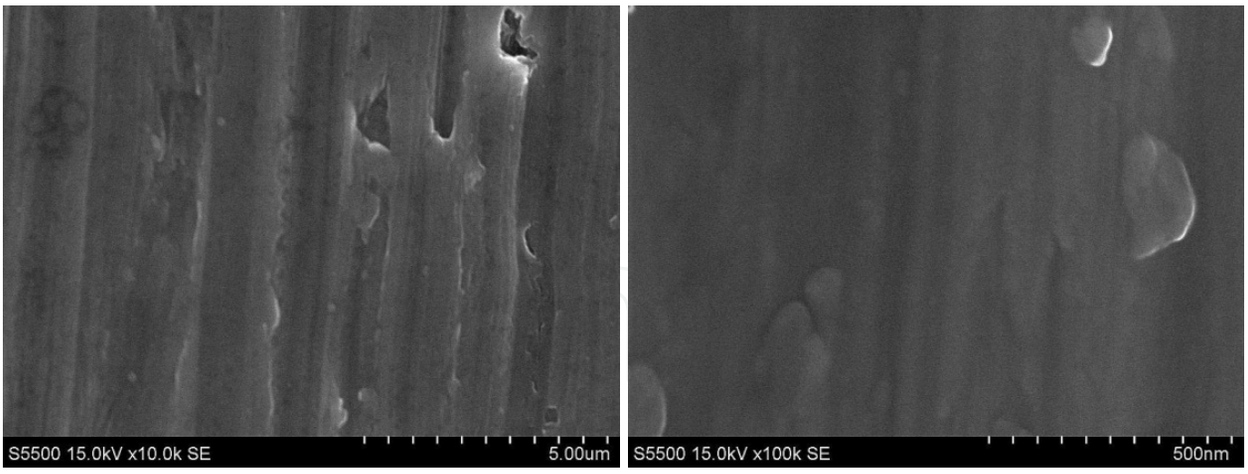

Figure 1. Surface morphology of Ti foil (initial sate, unmodified Ti).

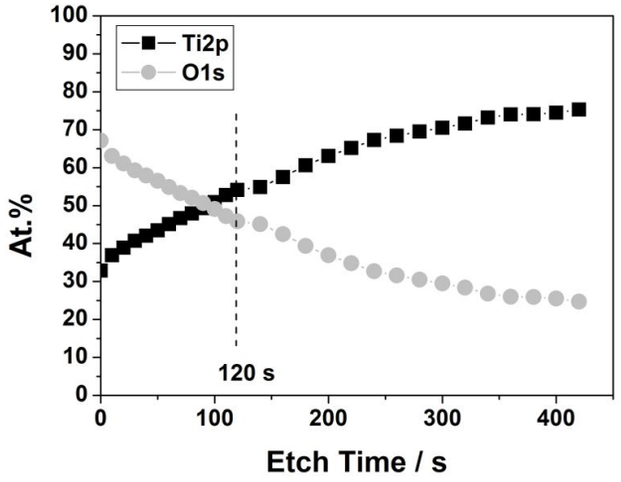

Figure 2. Normalized XPS profile for native oxide layer on Ti.

etch time	$Ti2p_{3/2}$ / eV	chemical state	atomic fraction / %
0s	454.2	Ti^0 (metal)	7
	456.1	Ti^{2+} (TiO)	6
	457.3	Ti^{3+} (Ti_2O_3)	8
	458.9	Ti^{4+} (TiO_2)	79
120s	454.2	Ti^0 (metal)	51
	455.7	Ti^{2+} (TiO)	15
	456.7	Ti^{3+} (Ti_2O_3)	20
	458.4	Ti^{4+} (TiO_2)	14

Table 1. $Ti2p_{3/2}$ binding energies as measured with XPS and suggested surface chemical species for native oxide layer on Ti before and after 120 s of Ar^+ sputtering.

In order to get an insight into the chemical state of titanium in the native oxide layer, XPS measurements were performed. The normalized XPS chemical composition profile is shown in Fig. 2. Table 1 presents binding energies of $Ti2p_{3/2}$ electrons for native oxide layer on Ti. The results show that TiO_2 is the main component of the passive layer (native oxide film).

However, some lower Ti-oxides are also present [51]. After 120 h of Ar^+ sputtering metallic Ti becomes the main component. In addition, the atomic fraction of the lower Ti oxides is higher than before sputtering. This could be a result of a TiO_2 reduction effects during sputtering, as already reported elsewhere [51].

Fig. 3 presents the schematic illustration of native oxide layer on Ti. Such kind of layer is spontanously formed in air on Ti surface and effectively protect metal surface against corrosion.

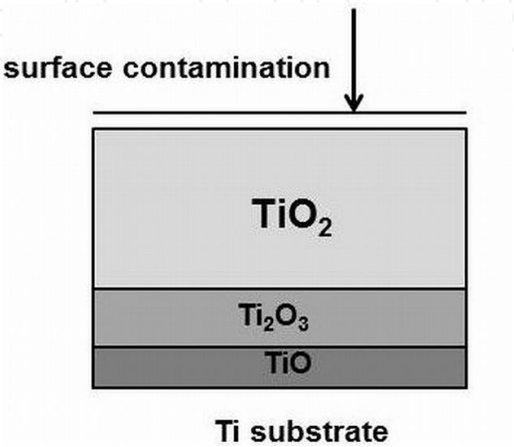

Figure 3. Schematic illustration of native oxide layer on Ti.

Results of accelerated corrosion resistance tests – called potentio-dynamic curves - (Fig. 4a, 4b) revealed that Ti exhibits a full resistance to local corrosion in the environment of 0.9% NaCl and artificial physiological solution (Hanks' solution) at pH ~ 7.0 [52]. An increase of current density on the polarization curves, within the region of the corrosion potential ~ 0.0 V up to 2 V, is not related to breakdown of the native oxide film but probably is due to growth

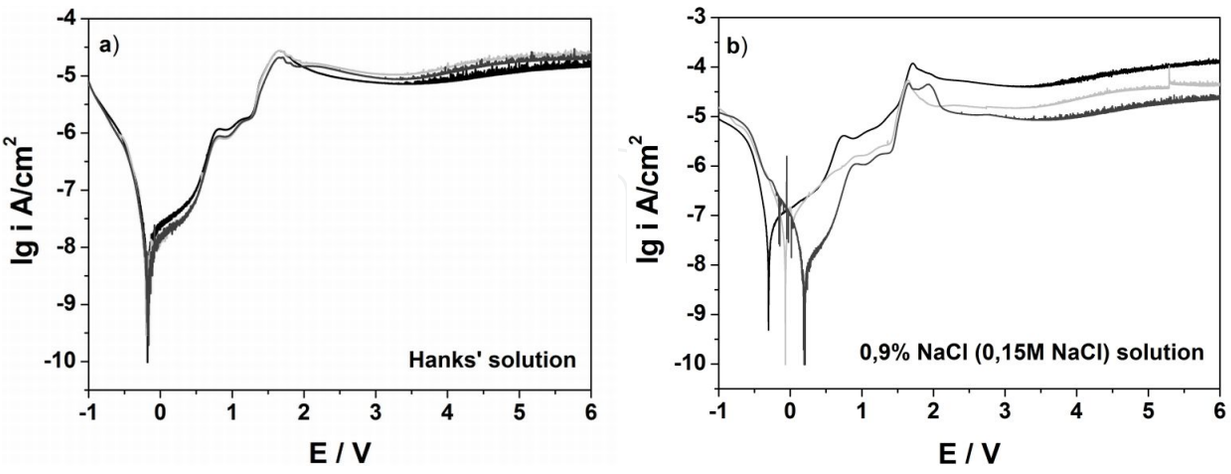

Figure 4. Potentiodynamic polarization curves of Ti (initial state) in Hanks' (a) and 0.9% saline solution. The curves were recorded at room temperature (25°C). An AutoLab PGSTAT 302N potentiostat/galvanostat were used in the standard 3-electrode configuration. A normal silver chloride electrode (Ag/AgCl (3M KCl)) and a platinum wire electrode were used as reference and counter electrodes, respectively. A slow potential sweep rate of 1 V/h was applied.

of an oxide layer. This involves also a simultaneous evolution of oxygen during polarization and anodic dissolution of titanium to Ti^{4+} ions [56]. At voltages higher than 2 V a stable oxide layer is formed (plateau in the range of 2 to 6V), in agreement with the analysis of thermodynamic equilibrium diagrams potential - pH for Ti (so-called Pourbaix diagrams [57]).

Preliminary corrosion tests of as-received Ti revealed that the material is resistant to corrosion in environments simulating physiological body fluids in a wide range of potentials. Further data indicate that the native oxide films on Ti allows for bone ingrowth to titanium implant surface REF. Such oxide films increase the biocompatibility of implanted elements reducing the activation of inflammatory reactions in the contact zone between metallic materials and living cells. In addition, a thin layer of protein, which covers the Ti surface, may significantly contribute to improvement of the biocompatibility of Ti [58]. This was confirmed in cell culture experiments (osteoblasts, U2OS). Fig. 5 shows fixed U2OS cells on the Ti substrate. It can be seen that the adsorption of albumin on the Ti surface significantly affects cell proliferation. Careful inspection of the living cells morphology revealed that the osteoblasts have well-developed nuclei (blue staining). The red staining corresponds to the cell membrane which exhibits the "dendritic structure". The characteristic shape of the cells and the presence of filopodia filaments suggest good cell adhesion to the Ti surface. Uniform distribution of the cells may ensure a good contact of the surrounding tissue with Ti implant [53,54].

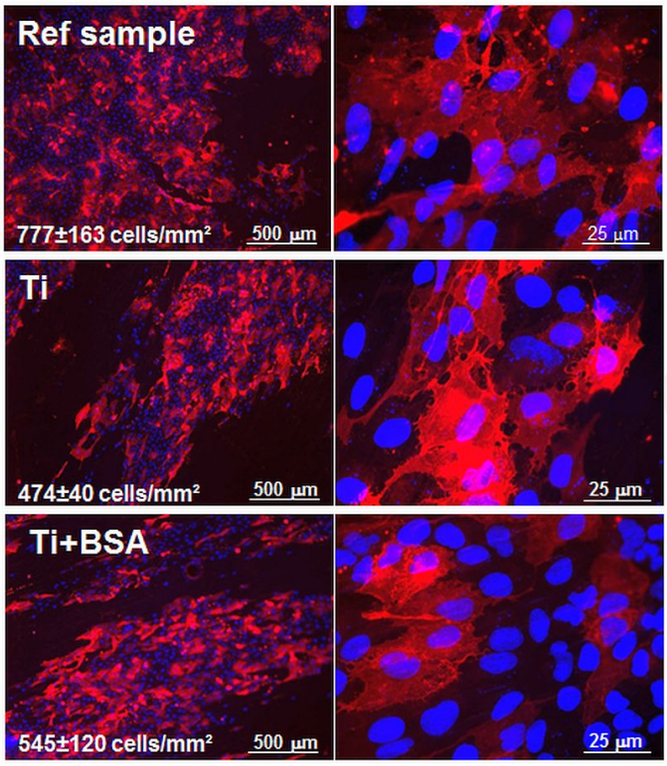

Figure 5. Fluorescent microscopy images of U2OS cells cultured for 48 h on pure Ti surface before and after albumin adsorption.

In the following step modification of Ti surface was performed in order to increase its biocompatibility. A two-step procedure (chemical etching or anodic oxidation of Ti followed by soaking in simulated body fluid or direct electrodeposition from Hanks' solution) was applied resulting in a fabrication of composite coatings on Ti which consist of porous titanium oxide layers and calcium phosphate phases.

At first porous titanium oxide layers with high specific surface area were fabricated.

Fig. 6 shows SEM images of a typical morphology of the Ti after chemical/electrochemical pre-treatment in different solutions. The SEM observation revealed that immersion in 3 M NaOH at 70°C for 24 h results in the formation of a 'coral-like' topography (Fig. 6a). The surface layer exhibits a developed, rough morphology characterized by a network of sharp-edged pores of various shapes. After pre-treatment in $H_2O_2 + H_3PO_4$ at room temperature, the morphology is quite different, and seems to be less developed (with shallower 'valleys') than that produced during NaOH pre-treatment. Fig. 6b suggests that Ti treated in $H_2O_2 + H_3PO_4$ exhibits sponge-like porosity. A distinct texture with round nano-sized pores is clearly seen. The nanopores are uniformly distributed across the surface [14]. The optimized anodization conditions applied resulted in the formation of TiO_2 nanotubes (hollow cylinders), at final voltage = 20 V for 2h, arranged perpendicularly to the substrate and separated from each other, Fig. 6c. The final voltage V_{max} has a strong impact on the diameter of the nanotubes, which changes from ~ 40 ± 10 nm at 10 V to almost 110 ± 10 nm at 25 V [22]. A detailed, mechanism of the formation and growth of self-organized TiO_2 nanotubes in electrolytes containing fluorides was recently proposed by Macak et al. [21,59] and Petukhov et al. [60]. Thermodynamic aspect of formation such kind of oxide layers was given by Wang et al. [61].

Atomic Force Microscopy - AFM was used to estimate the surface roughness of the samples under investigation [62]. As AFM resolution is limited by the radius of the tip, the AFM tip shape may result in a distorted representation of the actual surface micro-geometry. The parameters calculated from AFM data given in Table 2 may give an idea about the height of the 'hills' and the depth of the 'valleys' formed on the samples after the various surface treatments applied. The average roughness difference is evidenced by the R_q parameter. It should be noticed, however, that the roughness values reported in this paper are based on 1 μm × 1 μm AFM images, Fig.7. Before etching, the sample shows R_q of ~4.7 nm, whereas this parameter slightly increases up to ~5.1 nm for Ti($H_2O_2 + H_3PO_4$) and to ~6.3 nm for Ti(NaOH), respectively. The differences in R_a are small, with all values being in the range from 3.8 to 4.8. The R_z and R_{max} values, however, demonstrate a clear difference between the untreated and chemically pre-treated Ti samples. The highest values of those parameters are observed for Ti(NaOH) and indicate the presence of deep valleys, compare Fig 6a.

The as-grown porous anodic layers exhibited poor adhesion to the Ti substrate, so all the samples were annealed in air at 600°C for 2 h to improve their mechanical stability. After anodization process the samples have an amorphous structure. Fig.8 shows an SEM micrograph of TiO_2 nanotubes formed by anodic oxidation of Ti, after subsequent annealing. One can see that the heat treatment did not cause any distinct changes in the diameter of the nanotubes (see Fig.6c), but did modify the thickness of the oxide layer. Three distinct

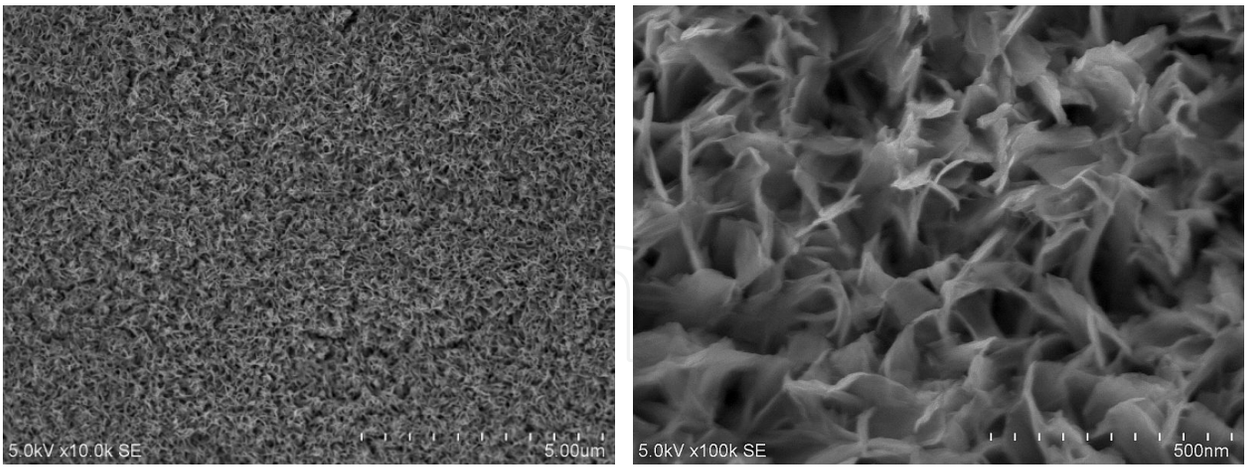

(a)

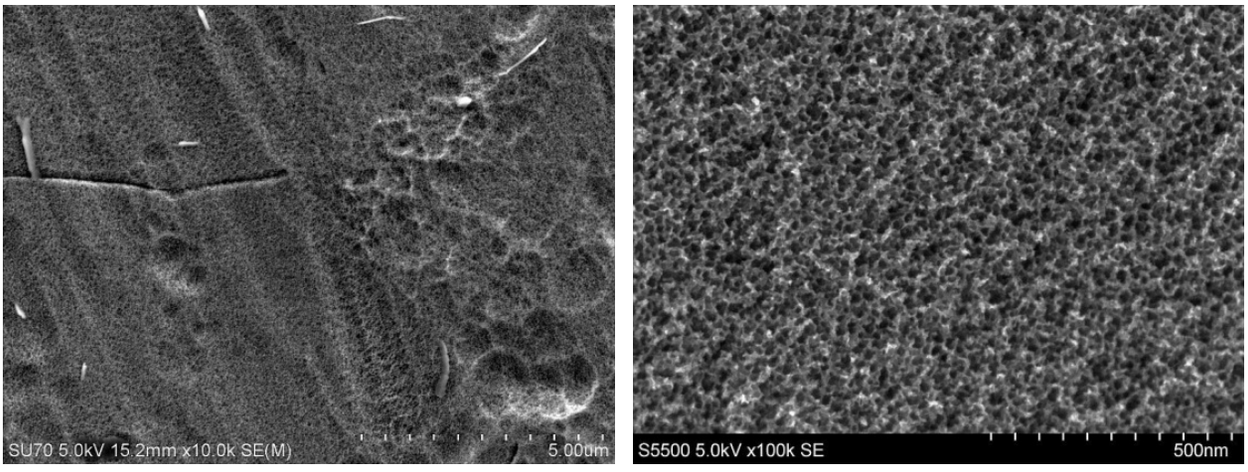

(b)

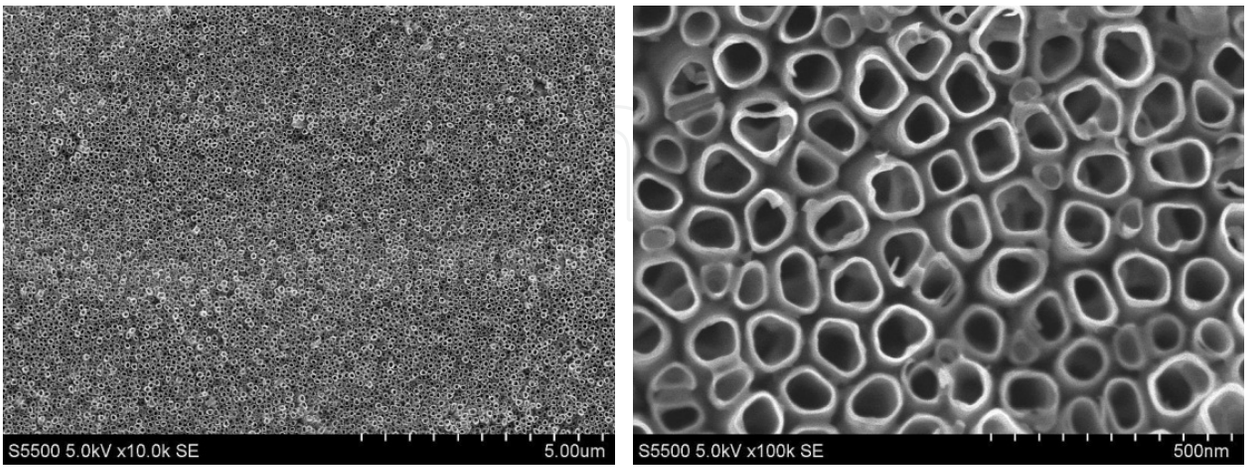

(c)

Figure 6. SEM images of chemically treated Ti in NaOH (a), H_3PO_4+H_2O_2 (b) solution and electrochemically treated in NH_4F+glycerol+water electrolyte (c).

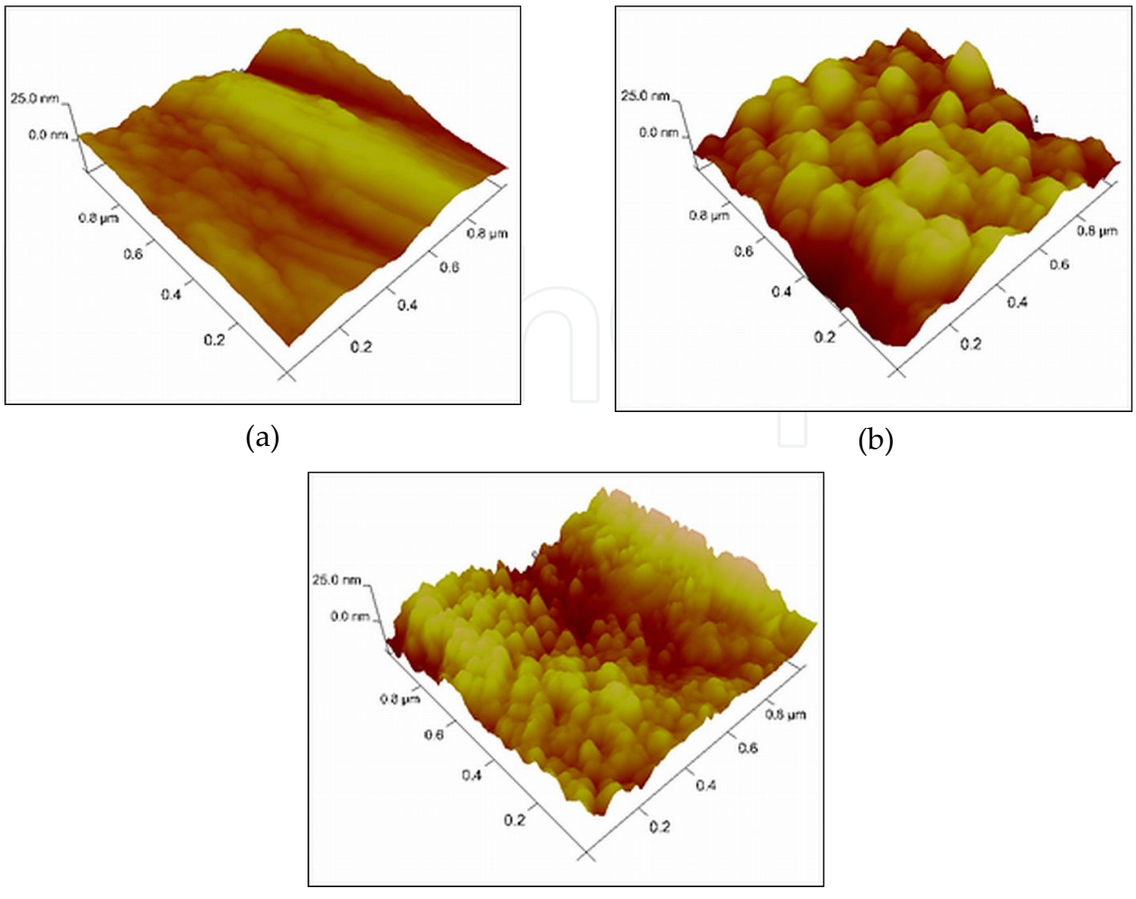

Figure 7. AFM images of untreated Ti (a) and chemically treated in NaOH solution (b), H_3PO_4+H_2O_2 solution (c)

samples	area	R_a (nm)	R_q (nm)	R_z (nm)	R_{max} (nm)
Ti (initial state)	1 x 1 µm	3,8	4,7	8,7	16,9
Ti (NaOH)	1 x 1 µm	4,8	6,3	14,1	26,2
Ti(H_3PO_4+H_2O_2)	1 x 1 µm	4,1	5,1	10,3	20,1

Table 2. Roughness parameter values for the Ti reference and Ti after chemical treatment in NaOH and H_3PO_4 + H_2O_2.

domains can be distinguished within the cross-section (Fig. 9): titanium dioxide nanotubes, an interphase region (a compact TiO_2 layer), and the titanium substrate [22]. TEM examinations revealed that the thickness of the whole oxide layer after heat treatment is about 1.3 µm (before annealing process ~0.8 µm) . The growth of the interphase region due to annealing causes an increase of thickhness of oxide layer, to ~0.5 µm. The intermediate zone is about three times thinner than the nanotube layer. This probably results from an additional oxidation of the Ti substrate and from a consolidation effect due to sintering of the nanotubes with the substrate due to the heat treatment in air [22, 63,64]. Fig.9 shows a high resolution STEM images of the intermediate zone (interphase region - compact TiO_2 layer) and single titanium dioxide nanotube after annealing at 600°C for 2 h.

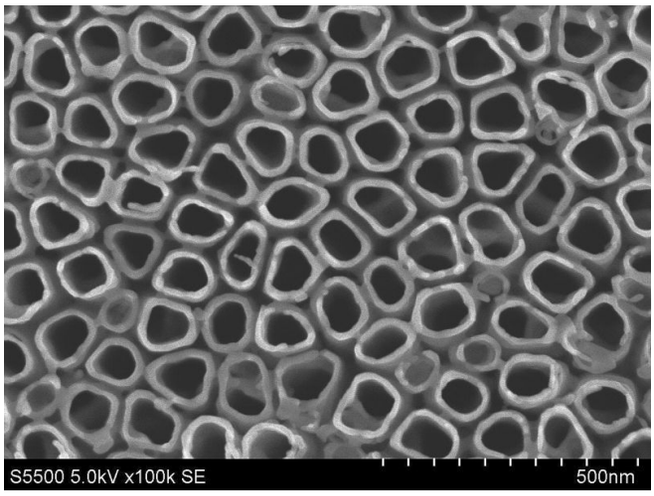

Figure 8. SEM image of the TiO_2 nanotubes after annealing in air at 600°C for 2 hours

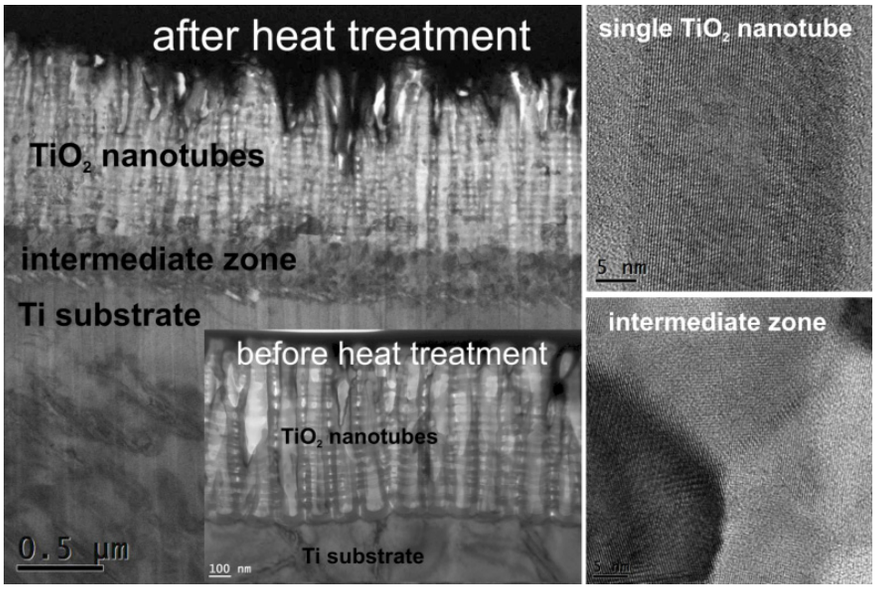

Figure 9. TEM image of a cross-section of the porous structure before and after heat treatment in air at 600°C, 2 h. High-resolution STEM images of the intermediate zone (interphase region) and singel TiO_2 nanotube.

The crystalline nature of the interphase region and the TiO_2 nanotubes is well visible. The lattice spacing for the nanotubes was measured to be circa 0.35 nm, which corresponds to the anatase phase (1 0 1) plane, where d = 0.352 nm (00-021-1272 JCPDS card number) [22]. XRD investigations of the sample annealed at 600°C showed a small amount of rutile phase, which may suggest the occurrence of a phase transition of anatase to rutile at this temperature [64,65], Fig.10. Our findings are in close agreement with those of J. Yu et al., and those of A. Jaroenworaluck et al. [63,65]. The authors suggest that the nucleation of the rutile phase takes place preferentially at the interface between the Ti substrate and the nanotube layer, which in turn suggests that the nanotubes maintain a stable tubular structure above the interfacial layer upon crystallization [64,65].

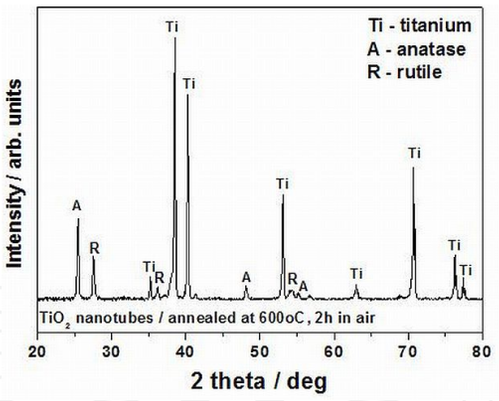

Figure 10. XRD spectrum of TiO_2 nanotubes formed on a Ti substrate after heat treatment.

Nanoindentation was conducted to probe the mechanical properties such as Young's modulus (Er) and nano-hardness (H) of nanoporous TiO_2 layer on a Ti substrate before and after annealing process. However, one should take into account that the parameters Er and H reflect not only the properties of the coating (below 1 μm thick), but are also influenced by the substrate. In addition the mechanism of interaction between indenter and the porous structure is not well understood. Crawford et al. have suggested that during indentation under loading the densification of nanotubes occurs as a result of heavy deformation [66]. In the same work the authors notice that an increased thickness of the porous layer may retard the build-up of stress needed to cause delamination during the loading cycle. This proposed mechanism seems to be also operative in our system.

The results show that the nano-hardness (H) of the annealed anodic porous layer is distinctly different from that of pure Ti and Ti after anodization process (as-received). Reduced elastic modulus Er and nanohardness H are higher for annealed nanotubes than for as-received ones. The nanotubes become hard and brittle due to annealing at 600°C in air, see Table 3. The observed changes of the mechanical properties relate to the effects of transition of the TiO_2 nanotubes structure from an amorphous to a crystalline phase (see, Fig. 11) and the formation of interphase region between oxide layer and Ti substrate due to heat treatment at 600°C in air. However, one should mention that after annealing at 600°C the TiO_2 nanotubes hardness is even lower than that of Ti metal, see Table 3. Our measurements for pure Ti are in good agreement with data presented by F.K.Mante et al. [67]. This interfacial zone detected by TEM (Fig.9) is probably responsible for the good adhesion of the TiO_2 nanotubes to the Ti substrate.

sample	E_R (GPa) ± ΔE_R	H (GPa) ± ΔH
TiO_2 nanotubes after anodization (as-received)	57.0 ± 3	1.3 ± 0.1
TiO_2 nanotubes annealed at 600°C in air for 1h	72 ± 5	1.8 ± 0.2
Ti foil, initial state	128 ± 4	3.0 ± 0.2

Table 3. Reduced Young modulus "Er" and nano-hardness "H"

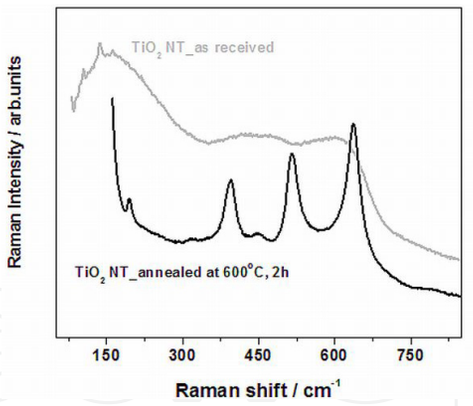

Figure 11. Normal Raman spectra of TiO_2 nanotubes: as-received and annealed at 600°C. In as-received state we can observed only a broad spectrum from amorphous TiO_2 structure. At 600°C the NR spectrum shows peaks around 635, 520, 390 cm^{-1}, which correspond to anatase phase. Our measurements for annealed TiO_2 nanotubes are in good agreement with data presented in the works [68,69].

TiO_2 nanotube structure offers a specific substrate for the development and optimisation of novel orthopedics-related treatments, with precise control over desired cell and bone growth behavior. As far as the effect of the diameter of the TiO_2 nanotubes is concerned, it was found that there were distinct size regimes for precisely controlling cell adhesion, cell morphology and/or the alkaline phosphatase (ALP) activity [2, 70]. It turns out that ~100 nm TiO_2 nanotubes, which induced the highest biochemical ALP activity of osteoblast cells, hold the most promise for the successful integration of orthopedic implant materials with the surrounding bone [2,70]. Considering the above discussion and Ref. [22],TiO_2 nanotube diameter was limited to 75±10 nm (20 V) or 110± 10 nm (25 V) for the purpose of our present studies.

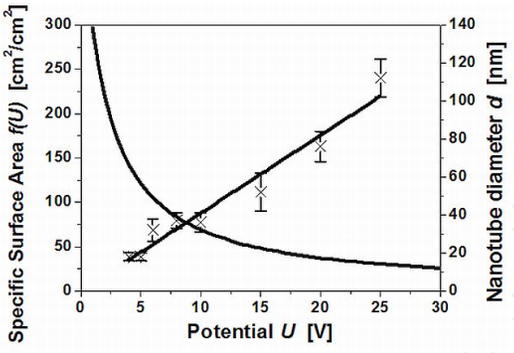

Figure 12. The relationship between the diameter of the titania nanotubes and the resulting specific surface area as calculated from the proposed geometric model (more details is given [71]).

The estimated surface area for TiO_2 nanotubes with an internal nanotube diameter of ~ 75 nm is ~150 cm^2/cm^2, while that for ~ 110 nm is about 250 cm^2/cm^2, see Fig. 12 As the calculations show, the specific surface area of a nanotubular structure increase with the nanotube diameter. In this context, the size of specific surface area for larger nanotubes is more promising for adhesion of proteins and living cells attachment. Higher specific surface area probably offers by higher population of active sites for nucleation of calcium phosphate coatings.

- **Deposition of Ca-P coatings by chemical or electrochemical methods from Hanks' solution**

The nucleation and growth of calcium phosphates (Ca–P) on titanium oxides has been extensively investigated because of its relevance to orthopedic applications [35,72]. A titanium surface can achieve direct bonding with bone tissue (osseointegration) through a very thin calcium phosphate layer. In recent years, intensive investigations have been conducted on the properties of both naturally and artificially formed titanium oxide layers to understand the positive effect of titanium oxide on bone bonding [11,33,53]. However, the mechanism is still not fully understood. Calcium phosphate bioceramics are considered to be more biocompatible than some other materials used for hard tissue replacement, because they more closely resemble living tissue in terms of composition.

For an artificial material to bond to a living bone, one requirement is the formation of a bonelike apatite layer on its surface in the body environment. The bone matrix into which implants are placed possesses its own intrinsic nanotopography. In particular, hydroxyapatite and collagen, which are the major building blocks of bone, expose to osteoblasts an extracellular matrix surface with a high roughness. The implant surface topography has been recently shown to influence the formation of calcium phosphate in simulated body fluid [73]. This phenomenon is related to the charge density and the topographical matching of the titania surface and the size of the Ca–P crystals found in bone [74]. However, it is to be expected that both the surface topography and the physicochemical properties of the surface have a cooperative influence on any surface precipitation reactions. Very few studies have been carried out where the combined effect of these parameters has been studied systematically [74-76]. The functional properties of titanium, especially its bone-binding ability can be improved through surface modification. Traditionally, hydroxyapatite has been used as a coating on the metal substrate to enhance bioactivity. Many coating techniques have been employed for the deposition of thin film coatings of hydroxyapatite, such as plasma spraying [27,77], electrophoretic deposition [78], sol–gel deposition [79] and electrochemical deposition [23,80]. In recent years, there has been increasing interest in the formation of a bioactive surface layer directly on the titanium substrate, which will induce apatite formation in the living environment or simulated body fluid (SBF) [81].

In our investigations, we attempted to use Ti oxides supports to provide a three-dimensional control over nucleation. Moreover, we were able to control the morphology and porosity - the size and number of the nucleation sites by using various methods of Ti oxidation (chemical etching, anodic poarization). The titanium oxide surface is predominantly negative in simulated biological environments (pH 7.4) and is consenquently electrostatically capable of attracting positively charged ions such as calcium. Cationic Ca^{2+} reacts then with negatively-charged PO_4^{3-} and CO_3^{2-} to form a Ca–P containing surface layer which eventually crystallizes to bone-like apatite [11]. Because this reaction takes place in an environment similar to that of natural apatite, it has been suggested [11] that such coatings may provide greater bone-bonding capability than those made by a conventional technique such as plasma spraying. One of the great advantages of a biomimetic method for coating metal implants with bone-like apatite layers over the commonly used plasma-spraying one

is that it imitates the mode in which hydroxyapatite bone crystals are formed in the body. The coatings thereby obtained are composed of small crystal units, which are more readily degraded by osteoblasts than are the large ceramic particles produced by plasma spraying [25].

In vitro mineralization studies are usually performed using simulated body fluids (SBFs) of similar composition to blood plasma. Among the most often used fluids are Hanks' balanced salt solution (HBSS) and Kokubo's (SBF). The main differences between HBSS and SBF are the degree of supersaturation in calcium and phosphate (lower in HBSS) and the presence of tris(hydroxymethyl)aminomethane (TRIS) buffer in SBF. Although SBF has a greater similarity with blood in terms of ionic concentration, the presence of TRIS buffer which forms soluble complexes with calcium ions, may be considered a disadvantage [82].

It is generally accepted that rough and porous surfaces could stimulate nucleation and growth of calcium phosphates. The surface topography is also known to strongly influence the wetting properties of materials [83,84]. The hydrophobicity of the surface plays an important role in the deposition of calcium–phosphate coatings from SBF or Hanks' solution. A hydrophilic surface is more favorable for initiating the formation of Ca–P [85]. The values of water contact angle for all the surfaces investigated are given in Table 4.

All morphologies obtained as a result of the chemical/electrochemical pre-treatments applied in this study, followed by simple immersion of the pretreated samples in a solution such as Hanks' medium (which is supersaturated with respect to the apatite), may be promising substrates for nucleation and the growth of calcium–phosphate coatings. Thus, this is the first step, which should be performed prior to the formation of a calcium phosphate layer on the modified Ti substrate.

samples	contact angle
Ti	77 ± 5
Ti(H_3PO_4+H_2O_2)	57 ± 5
Ti(NaOH)	27 ± 3
TiO_2 NT (HT)	3 ± 1

Table 4. Water contact angle values for surfaces under investigation

The nucleation and growth of apatite on chemically/electrochemically pre-treated Ti depends not only on surface characteristics such as topography/morphology, but also on the chemical composition and chemical state of the elements present on the surface. In order to get an insight into the chemical state of titanium before and after the chemical treatments applied, XPS measurements were performed.

Table 5 provides the binding energies of Ti $2p_{3/2}$ and O 1s electrons for all the samples investigated. In all cases, the pre-treated Ti surfaces exhibited a clear O 1s signal at 530.1–530.5 eV, ascribed to the Ti–O bond due to the presence of titanium oxide at its surface. The results confirm that TiO_2 is the main component of the chemically/electrochemically pre-treated Ti surface. Deconvolution of the Ti 2p signals suggests that some lower Ti-oxides are

also present for the chemically pre-treated samples (see Table 5). Our XPS investigations do not suggest the presence of Ti–OH bonds on the Ti reference, Ti(NaOH), Ti(H_3PO_4 + H_2O_2) or TiO_2 NT substrates [14,22]. Some authors have reported [13] that the presence of hydroxyl groups on the surface is crucial for calcium titanate formation, which then incorporates PO_4^{-3} groups and converts into apatite. The authors believe that the Ti–OH containing species, notably unstable $Ti(OH)_4$, may only be formed in situ, in simulated body fluid, or in vivo, in the presence of blood plasma [13]. Recently, it was found that titanium metal and its alloys, when subjected to successive NaOH aqueous solution and heat treatment, show apatite-forming ability and integrate with the living bone after implantation. This apatite-forming ability is attributed to the amorphous sodium titanate formed during the treatments [15,17]. Interestingly, the H_2O_2 + H_3PO_4 pre-treated sample produced an oxide film which also contains phosphate ions (see Table 5). A possible incorporation of phosphate ions into the oxide film may provide a compositional basis facilitating the formation of calcium phosphates – primary inorganic phases of bone – which have osteoinductive properties in physiological fluids [14].

	Ti2p3 / eV	**P2p3 / eV**	**O1s / eV**	**chemical state**
Ti(NaOH)	**459.0** 457.6		**530.5**	**TiO_2 (major component)** Ti_2O_3 (minor component)
Ti(H_3PO_4+H_2O_2)	458.6 456.5	 133.0	530.1 531.7	**TiO_2 (major component)** TiO (minor component) phosphate, PO_4^{3-}
TiO_2 nanotubes	458.9		530.4	**TiO_2 (major component)**

*Ti in TiO_2 – 458.8 eV, Phosphates (132.0 – 133.0 eV), Handbook of X-ray Photoelectron Spectroscopy, A Reference Book of Standard Spectra for Identification and Interpretation of XPS Data, Edited by Jill Chastain, Roger C. King, Jr, Physical Electronics, Inc., USA, 1995

Table 5. Ti $2p_{3/2}$, O 1s and P $2p_{3/2}$ binding energies as measured from corrected XPS spectra before and after chemical/electrochemicall pre-treatment, and surface compounds evaluated using a deconvolution procedure.

- **Morphology, structure and chemical composition of deposited Ca-P coatings (HR-SEM, AES, XPS, FTIR)**

Having obtained stable Ti oxide substrates we further attempted to functionalize them by means of a calcium phosphate overlayer. The results are discussed below.

As the SEM investigations show, soaking chemically pre-treated Ti surfaces in Hanks' solution at 37°C for 7 days produced calcium phosphate coatings of similar morphology (Fig. 13 a and b). Individual and clustered ball-like particles on top of a compact Ca–P layer containing numerous submicron features are well visible. This type of developed morphology is similar to that reported in the literature [12,14, 18, 22, 80]. After immersion for 7 days, the TiO_2 nanotubes are coated with a denser layer which is composed of spheroidal particles tightly packed together. Some single and clustered ball-like particles of about 0.5–1.0 μm in diameter are also present on the surface. The higher magnification micrographs indicate that those features have a cauliflower-like structure composed of

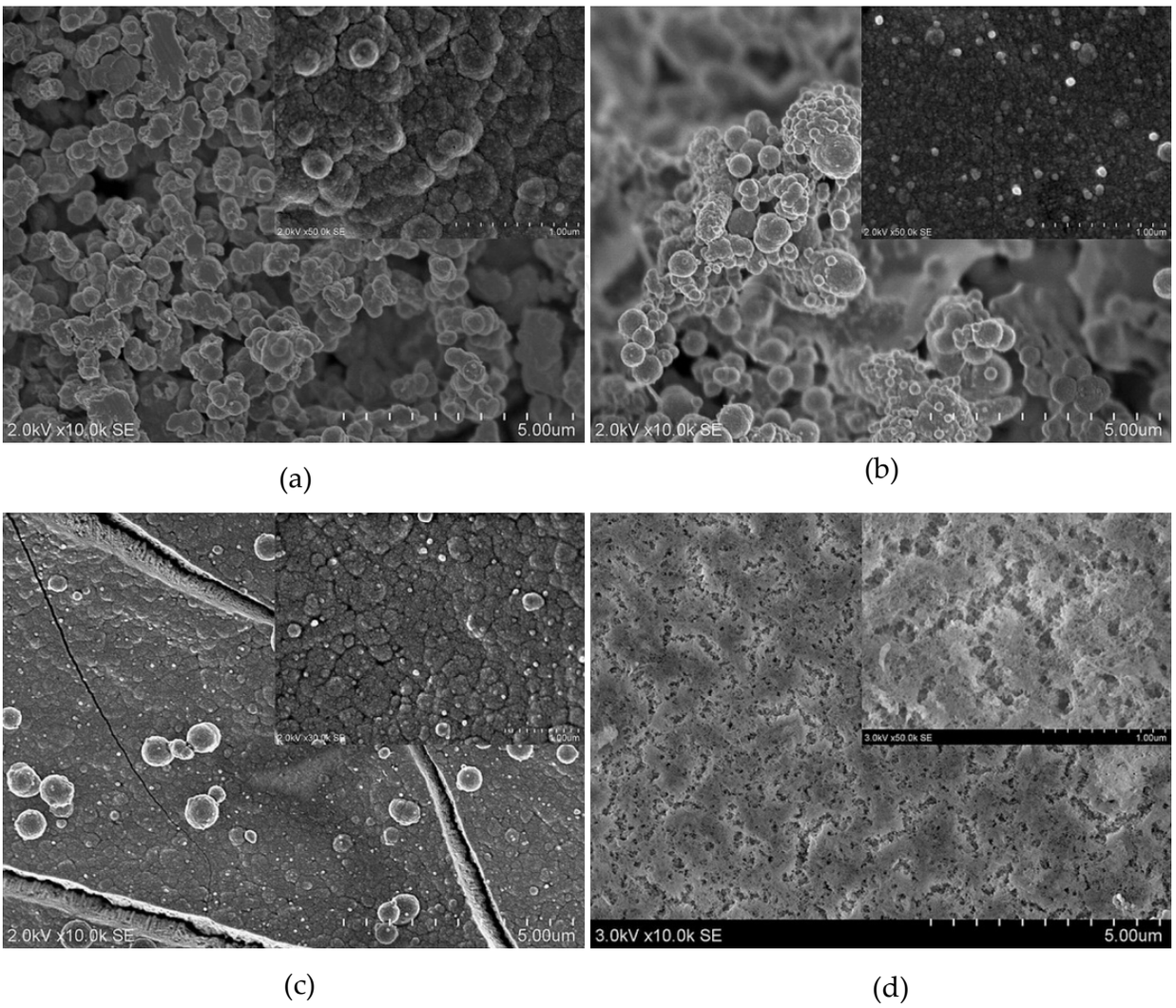

Figure 13. SEM images (top view) of Ti after chemical/electrochemical treatment and after subsequent immersion in Hanks' solution – 7 days, temperature 37°C : a – NaOH, b – H_3PO_4+H_2O_2, c – TiO_2 nanotubes. SEM image of the electrodeposited Ca-P coating on a Ti from Hanks' solution (d).

many small crystallites, as shown in Fig. 13c. The Ca-P coating formed on TiO_2 nanotubes seems to be better crystallized than on Ti chemically pretreated in alkali and acidic solutions. Our SEM examinations reveald that electrodeposited calcium phosphate coating exhibits a completely different morphology characterized by a network of longitudinal pores of different shapes (Fig. 13d).

Fig. 14 shows a cross-sectional view of the calcium phosphate coating on Ti(NaOH) and TiO_2 NT samples. The Ca–P coating on etched Ti is well integrated within the porous TiO_2 layer (in fact a Ca–P/Ti oxides/Ti composite is formed), which may improve the bonding of the coating to the pre-treated Ti substrate, Fig. 14a. Fig.14b clearly indicates that Hanks' solution penetrates the interior of the nanotubes and the spaces between individual TiO_2 nanotubes. Deposition of the calcium phosphate coating on the surface of the nanotubes by soaking leads to the formation of a specific composite-like layer. An intermediate zone is thus formed with TiO_2 nanotubes and phosphates mutually "permeating" each other. The

vertically aligned TiO_2 nanotubes on Ti substrate act as an intermediate layer for improving the binding between apatite coating and Ti substrate, and for providing a mechanical stability of the whole composite. One may anticipate that a Ca–P deposit on a TiO_2 porous layer may promote early bone apposition and implant fixation by enhancing the chemical bonding between the new bone and the surface of those materials [14,22].

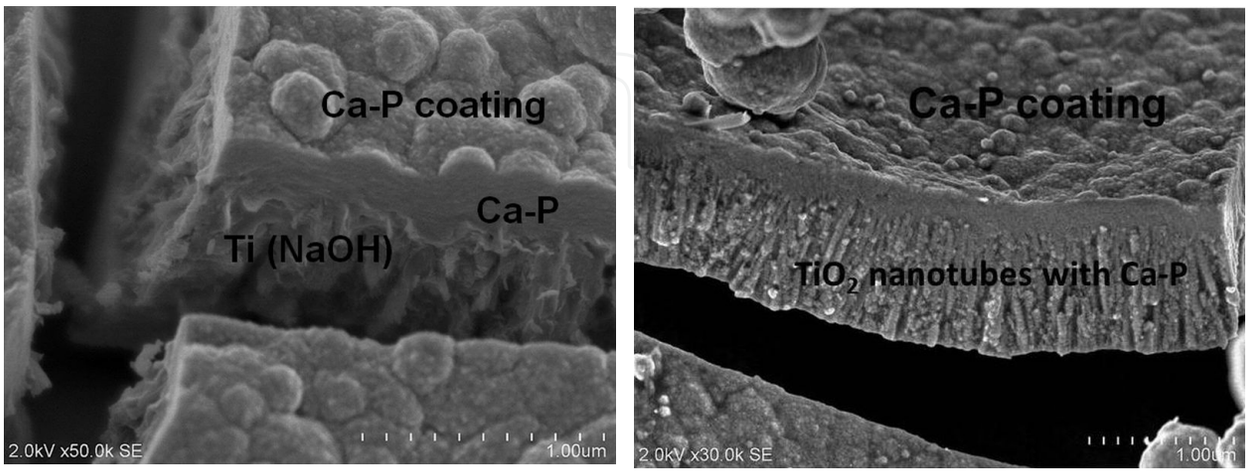

Figure 14. SEM images of a cross-section of the titanium oxide porous structure with a deposited calcium phosphate coating.

Fig. 15 shows a STEM cross-sectional view of the Ca-P layer after electrodeposition process. The thickness of the electrodeposited layer is about 200 nm. The high resolution STEM images of the Ca-P coatings suggest that electrodeposition from Hanks' solution at the potential – 1.5V vs OCP leads to the formation of homogenous layer with good adhesion to the substrate.The high resolution STEM image shows a subtle porosity of the Ca-P layer. Well visible nanopores are uniformly distributed across the "sponge like structure" with a

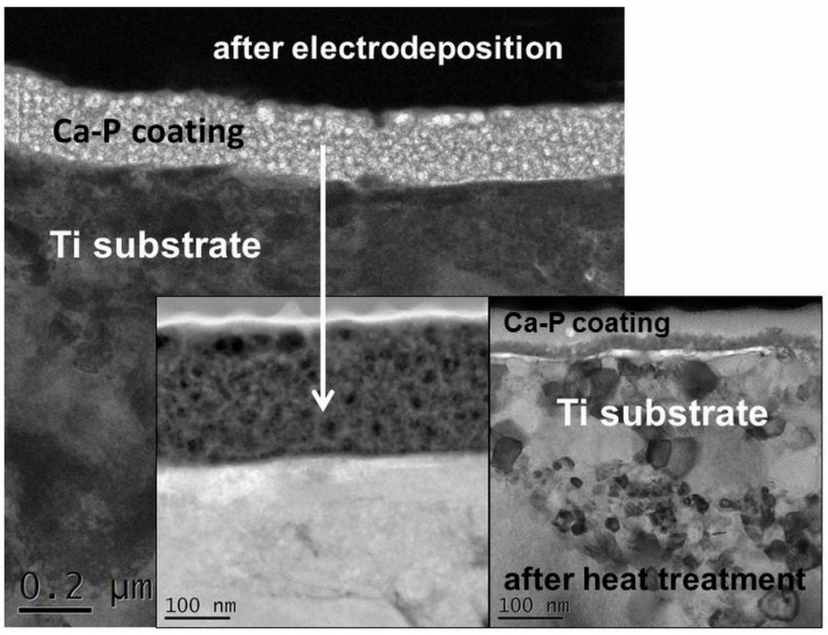

Figure 15. STEM images of the electrodeposited Ca-P coatings before and after heat treatment.

gradual change of the pore size with depth. Larger pores within the uppermost layer may assure better integration with bone. Nanoindentation technique allowed the coating's hardness and reduced Young's modulus to be measured with a load of indenter - 1 mN.

Such a low load did not cause the breakdown of the Ca-P layer by the indenter. The hardness of the coating was determined at the level of ~ 0.2 GPa, see Table 6. Thermal treatment was applied to increase the hardness of the electrodeposited coating and to check the influence of temperature on the size of the pores present in the layer. TEM revealed that the thickness of the Ca-P coating after heat treatment is about four times lower than that obtained for the sample after direct electrodeposition (without heat treatment). Three distinct domains can be distinguished within the cross-section (Fig. 15): Ca-P coatings, an interphase region (gray layer), and the titanium substrate. An increase of the hardness of about 6 GPa and Young's modulus to ~ 143 GPa was observed after heat treatment in 700^{o}C for 1 h in air. The values obtained are comparable to the hardness of the layers fabricated by pulse laser deposition method [86]. Such increase is probably related to the change of the structure of electrodeposited layer (solid homogeneous Ca-P layer was formed separated from the Ti substrate with a thin transition zone), and internal structure of the substrate during heat treatment. Ti grains of size below 100 nm could be observed after heat treatment, see Fig.15. The grain size reduction is probably related to recrystallization process during annealing. The change of the electrodeposited Ca-P coating structure also contributes to the increase of the mechanical properties of the investigated system (even in relation to the unmodified Ti). Such phenomenon was not observed for anodically polarized layers subsequently annealed at 600^{o}C in air, see Table 3.

sample	E_R (GPa) ± ΔE_R	H (GPa) ± ΔH
Ti (initial state), Ti foil	127.8 ± 5.5	4.7 ± 0.5
Ti with electrodeposited Ca-P coating	25.4 ± 2.7	0.17 ± 0.03
Ti with electrodeposited Ca-P coating after annealing at 700^{o}C, 1h in air	143.1 ± 6.1	6.4 ± 0.4

Table 6. Reduced Young modulus "Er" and nano-hardness "H" for electrodeposited Ca-P coatings before and after heat treatment.

Auger electron spectroscopy (AES) technique was used to control the local chemical composition of the Ca-P coatings. AES analysis revealed the presence of P, Ca, O, Mg, and C in the layer. Qualitatively, similar chemical composition of the Ca-P coatings was obtained using chemical/electrochemical methods, see Fig.16.

XPS analysis revealed that the surface is enriched in calcium and phosphorous, with Ca/P molar ratios of 1.08 (NaOH solution), 1.09 (H_2O_2 + H_3PO_4), 1.10 (electrodeposited layer) and 1.37 (TiO_2 nanotubes), Fig. 17. This is less than the stoichiometric hydoxyapatite ratio of 1.67. However, our EDS results show that the atomic concentration ratio of Ca/P is higher for the all samples. In case of bulk sample the EDS technique provides information with a lateral resolution of ~ 1 μm and depth resolution of ~ 2-3 μm. It is noteworthy that XPS measurements provide surface information from the few uppermost nanometers of the samples. This suggests that a

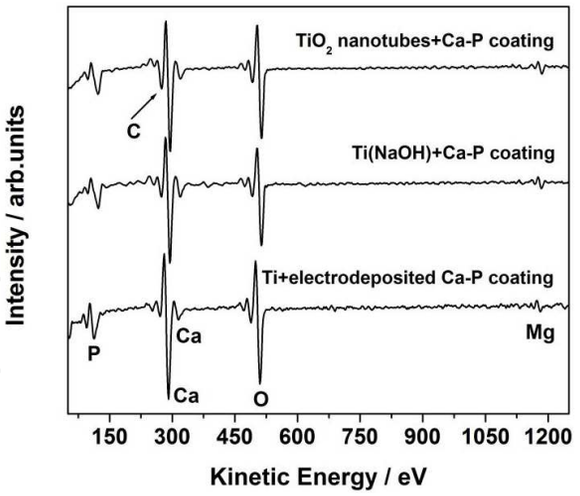

Figure 16. AES survey spectra recorded on the surface of Ca-P coatings obtained from Hanks' solution.

nucleation of calcium phosphates phases with lower Ca/P ratio is limited to the outermost surface only. This observation does not concern calcium phosphate layers obtained on TiO_2 nanotubes (Ca/P = 1.37). The differences in the morphology and crystallinity of the titanium oxide layers fabricated by chemical etching and anodic polarization are likely to play a role here [14, 22, 87]. The differences in the molar Ca/P ratio may result from different formation stages within the bulk comparing to those in the outermost layer of the coating. Some authors suggest that amorphous calcium phosphate (ACP ($Ca_x(PO_4)_y \cdot nH_2O$), Ca/P=1.2–2.2 [35]) is transformed in vitro into octacalcium phosphate (OCP ($Ca_8(HPO_4)_2(PO_4)_4 \cdot 5H_2O$), Ca/P=1.33 [35]) which, in turn, evolves into hydroxyapatite; at lower pH values, the intermediate phase seems to be dehydrated dicalcium phosphate (DCPC ($CaHPO_4 \cdot 2H_2O$), Ca/P=1) [35]. Our results bolster this suggestion. The estimated molar Ca/P ratio by EDS measurements suggest formation of octacalcium phosphate (OCP, Ca/P = 1.33), and probably some intermediate Ca–P phases [88]. The OCP compound is thought to be a precursor for the crystallization of bone-like apatite/hydroxyapatite [89].

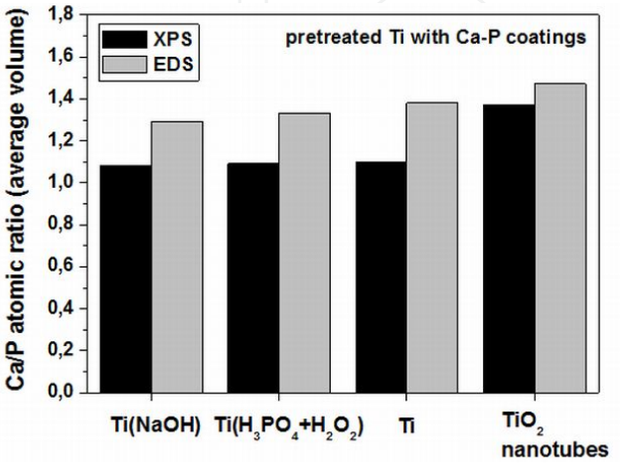

Figure 17. Results of the XPS and local EDS analysis (Ca/P atomic ratio) of calcium phosphate coatings electrodeposited on pure Ti or deposited on chemically/electrochemically treated Ti.

Careful inspection of the chemical composition near the uppermost layer revealed that Ca/P molar ratio changed within the Ca-P coating depth. Fig.18 presents partial compositional profile (the relative Ca/P atomic concentration) of electrodeposited layer on Ti, as measured using XPS combined with ion sputtering. As seen from the results presented in Fig.17, the Ca/P concentration ratio is distinctly higher within the layer than at the surface. After 300 s of etching (which corresponds to a thickness of about 12 nm, based on a sputtering rate 0.04 nm/s) the Ca/P atomic ratio is close to 1.43. This later finding correlates with the results of EDS measurements (1.38, see Fig.16). After 600 s of sputtering the Ca/P atomic ratio remains on the same level; apparently the chemical composition does not change further with depth. The differences in the molar Ca/P ratio between the bulk and the outermost layer of the coating, is distinct.

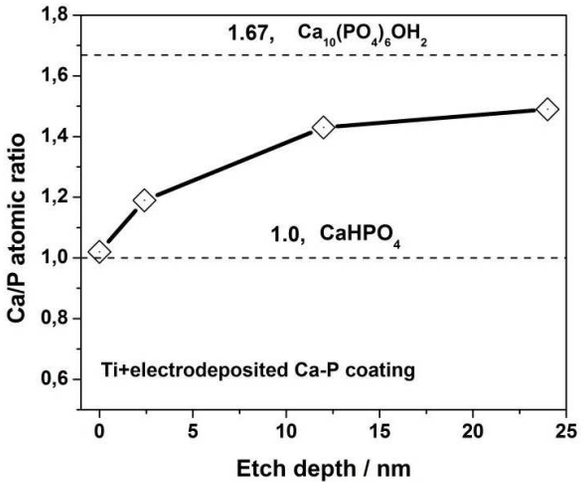

Figure 18. Composition of Ca/P concentration ratio vs. sputtering depth for a coating electrodeposited on Ti.

Table 7 shows the binding energies of the O 1s, Ca $2p_{3/2}$, and P $2p_{3/2}$ signals, and the suggested chemical composition of the biomimetic coatings. Position of the main peak of P $2p_{3/2}$ may change within a range of 132.6-133.4 eV for all coatings. The spectral data for Ca suggest the presence of calcium phosphate groups (Ca $2p_{3/2}$: 347.5 - 347.9 eV). The main component of the O 1s peak at BE = 531.1 - 531.6 eV is attributed to PO_4^{3-} groups. The results show that all coatings containing calcium phosphates groups, which are formed on the chemically/electrochemically treated Ti substrate [14, 22].

Fourier transform infrared (FTIR) spectroscopy was used to obtain additional information on the chemical composition of the Ca–P coatings. Hydroxyapatite, the main mineral component of biological bone, absorbs IR radiation due to the vibrational modes from the phosphate and hydroxyl groups. In biological apatites, some PO_4^{3-} ions are substituted by CO_3^{2-} ions, and the IR technique is very sensitive to these carbonate substitutions, so even a small amount of carbonate can be detected [90]. Table 8 shows the results of the FTIR investigations for calcium phosphate coatings formed on chemically/electrochemically treated Ti or on a pure Ti. The ν_4 bending vibrations of PO_4^{3-} are detected circa 560 cm^{-1}, although the spectra are dominated by the ν_3 stretching PO_4^{3-} vibration mode in the 1000–1100 cm^{-1} range. Bands for

Ti surface modification	Ca2p$_{3/2}$ / eV	P2p$_{3/2}$ / eV	O1s / eV
NaOH pretreatment + immersion in Hanks' solution 7 days	347.5 – 347.9 / Ca^{2+}	132.6 – 133.4 / PO_4^{3-}	531.1 – 531.6 / O^{2-}
H_3PO_4 + H_2O_2 + immersion in Hanks' solution 7 days			
after direct electrodeposition in Hanks' solution (- 1.5 V vs. OCP)			
anodic oxidation pretreatment (20 V) + immersion in Hanks' solution 7 days			

*on the measured surfaces we also detected: $CaCO_3$, HPO_4^{2-}, $CaCl_2$

Table 7. Ca 2p$_{3/2}$, P 2p$_{3/2}$ and O1s binding energies as determined from corrected XPS for Ca-P biomimetic coatings, and surface compounds evaluated using a deconvolution procedure.

ν_3 vibrations of C–O mode appear, along with a well-defined bands at 870 – 875 cm^{-1} (ν_2 vibrations of C–O) known to be specific for a carbonated apatite in which PO_4^{3-} ions are substituted by CO_3^{2-} ions [91]. However, the characteristic peaks at the range 870 – 875 cm^{-1} and 959 cm^{-1} suggest the presence of HPO_4^{2-} as well [92]. The OH bands at about 630 cm^{-1} and at about 3570 cm^{-1} are absent for the all coatings. Some authors have attributed these missing OH modes to a perturbation of the hydroxyl stretching and bending modes on the apatite surface by the hydrogen bonding of water molecules to the surface OH^- ions [93]. The absence of the OH^- vibration at 3570 cm^{-1} may also suggest that carbonate substitutes for OH^-. However, there is no

Ti surface modification	ν_4, PO_4^{3-}	ν_3, PO_4^{3-}	HPO_4^{2-}	ν_3, C-O	ν_2, C-O, CO_3^{2-}
NaOH pretreatment + immersion in Hanks' solution 7 days	560 – 562 cm^{-1}	1000 – 1100 cm^{-1}	870 – 875 cm^{-1}, 959 cm^{-1}	1460 – 1490 cm^{-1} 1420 cm^{-1}	870 – 875 cm^{-1}
H_3PO_4 + H_2O_2 + immersion in Hanks' solution 7 days					
after direct electrodeposition in Hanks' solution (- 1.5 V vs. OCP)					
anodic oxidation pretreatment (20 V) + immersion in Hanks' solution 7 days					

*H_2O (3000 – 3500, 1630 – 1650 cm^{-1})

Table 8. Results of the FTIR investigations. Identification of the chemical compounds.

evidence that CO_3^{2-} substitutes for OH^-, since the characteristic absorption band at 1545 cm^{-1} associated with this type of substitution was not observed. The above discussion suggests that chemically pre-treated surfaces are a favorable substrate for the deposition of an apatite-like coating [14, 22].

- **Biological response**
  a. Protein adsorption (BSA)
  b. Cell culture experiments (U2OS)

Hydroxyapatite (HA) and calcium phosphate coatings (Ca–P) have been used primarily to alter implant surfaces, on the assumption that the osteointegration of the implants can be improved. However, the processes occurring at the bone/implant interface are still not fully understood; in particular, the role of biomolecules and their influence on initial bioadhesion and coating dissolution has received little attention. When a biomaterial is implanted into the body, its surface is immediately covered with blood and serum proteins. The presence of an adsorbed protein layer mediates cellular responses to the implants [94]. It is expected that, as proteins from biological fluids come in contact with biomimetic surfaces, cellular adhesion, differentiation and extracellular matrix production may be affected. Cell adhesive proteins, found at high concentration in blood, can provide attachment sites for osteoblast precursors binding to the implant, which then leads to faster in-growth of bone and stabilization of the implant. Elsewhere, the surface properties and structures of the materials play an important role in the adsorption of proteins. Surface chemistry and topography are the most important parameters affecting biological reactions [54,95]. The effects of surface topography on protein adsorption and cell adhesion have been extensively investigated by other authors [54,83,96]. The chemical composition of the substrate surface strongly affects the protein adsorption process, as has been documented [53,97].

To evaluate the potential application of our materials for biomedical implants, we examined protein adsorption on the surfaces studied. Serum albumin (SA) was used as a model in this study, as it is the most abundant protein in blood.

Typical XPS spectrum of the Ca-P coating after 20 min incubation in PBS solution containing BSA at 37°C revealed the presence at the surface of Ca, P, O, C and weak signal for Mg and Na. After protein adsorption, a new XPS peak around 400 eV appeared which corresponds to nitrogen, Fig.19. This signal was attributed inter alia to amide groups in albumin molecules. In contrast, the signals from Ca and P are not well visible, suggesting that the surface is completely covered by the protein layer.

Table 9 presents the binding energies of the C1s and N1s XPS signals and the suggested chemical state of the detected elements after protein adsorption on the Ca-P coatings. The XPS reference data for pure BSA are also given. The N1s high-resolution XPS spectrum indicates the presence of N-C=O, C-N, and N-H characteristic protein functional groups at ~ 400.0, ~ 398.0 and ~ 402.0 eV, respectively [22,95,98,99]. XPS signals from the carbon species expected from the bases (C backbone) included the main hydrocarbon, carbon bound to nitrogen or oxygen, amide carbon and carbon double bounded to oxygen [14, 22,95,98,99]. This suggests that the protein molecules are adsorbed on the calcium phosphate coatings.

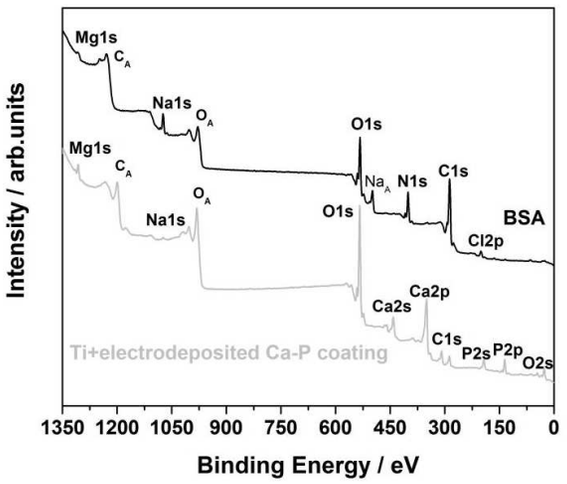

Figure 19. XPS survey spectra before and after adsorption of BSA protein on electrodeposited Ca-P coating on a Ti.

	C1s / eV	N1s / eV	type of bonds
Albumina, ref sample	288.2	400.2	N - C=O
		398.6	C – N
		402.1	N – H
	285.0		C-C / C-H
	286.6		C-O / C-N
	290.0		C=O
NaOH pretreatment + immersion in Hanks' solution 7 days	288.1 – 289.2	399.9 – 400.2	N - C=O
H_3PO_4 + H_2O_2 + immersion in Hanks' solution 7 days		398.1 – 398.5	C – N
		401.9 – 402.0	N – H
anodic oxidation pretreatment (20 V) + immersion in Hanks' solution 7 days	285.0		C-C / C-H
	286.2 – 287.4		C-O / C-N
after direct electrodeposition in Hanks' solution (- 1.5 V vs. OCP)	289.9*		C=O*

*Only for electrodeposited sample

Table 9. C1s and N1s binding energies as measured with XPS and suggested surface chemical species for all samples after protein adsorption.

FTIR results of BSA adsorbed on the calcium phosphate coatings are presented in Table 10. BSA was found to interact with the surfaces studied. The main bands in the range 1650 – 1655 and 1520 – 1540 cm^{-1} have been assigned to amides I and II, respectively [14, 100,101]. Our findings are in good agreement with the measurement for the pure albumin, used as reference sample (Fig. 20) and confirm previous results obtained by XPS method.

	Amide I (C=O)	Amide II (N-H)
Albumin, ref sample	1655 cm^{-1}	1535 cm^{-1}
NaOH pretreatment + immersion in Hanks' solution 7 days	1650 – 1655 cm^{-1}	1520 – 1540 cm^{-1}
H_3PO_4 + H_2O_2 + immersion in Hanks' solution 7 days		
anodic oxidation pretreatment (20 V) + immersion in Hanks' solution 7 days		
after direct electrodeposition in Hanks' solution (-1.5 V vs. OCP)		

*Resolution 4 cm^{-1}

Table 10. Position of the main bands: Amide I and Amide II for serum albumin adsorbed on the biomimetic Ca-P coatings.

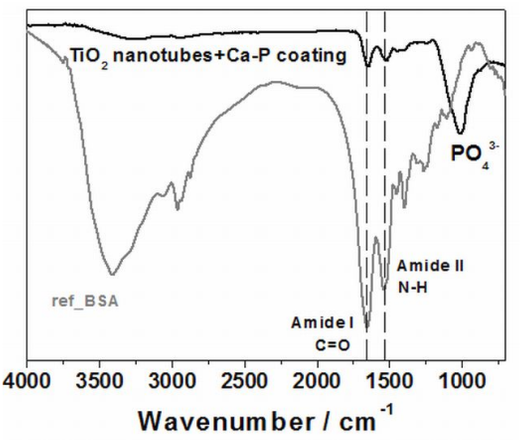

Figure 20. FTIR spectrum of TiO_2 nanotubes coated with calcium phosphate (Ca–P) after 7 days' immersion in Hanks' solution. Reference spectrum for pure albumin is also given.

Data reported [102,103] in the literature suggested that BSA may have a specific binding interaction with apatite/ hydroxyapatite and thus result in an improvement in the bioactivity for osteoblast cells with regards to their adhesion and proliferation. These findings, taken in relation to present results, suggest that it might be possible to develop better Ca–P-based biomaterials through an incorporation of albumin into the mineral matrix to improve cell adhesion and proliferation [102-104]. Our preliminary results of the response of human osteosarcoma U2OS cells to the surfaces investigated are in qualitative agreement with the protein adsorption measurements. Fig. 21 shows the cells on Ti with electrodeposited Ca-P coatings before and after adsorption of BSA proteins. Fluorescence microscopy observations revealed that the amount of U2OS cells after 72 h of incubation is distinctly higher on the Ca-P coating with adsorbed albumin than for the sample without proteins. A series of investigations performed by Yamaguchi and coworkers have suggested

that albumin is released by osteoblast cells present in fracture healing sites and this excess albumin increases proliferation of the surrounding cells. In our study, the surface modification with BSA led to significant improvement in osteoblast-like cells binding to an electrodeposited Ca-P coating. Similar observation, but for MC3T3-E1 cells were reported by other authors [102-104], who have found that adsorption of BSA to the surface of conventional and nanophase ceramic (including hydroxyapatite) influences the activity of adherent cells. After 120 h of incubation, however, the increase in cell number is observed only for surface without BSA. Such a result could be expected. Usually a longer time of incubation increase probability of proliferation of living cells. The adsorption of BSA probably affects positively the kinetics of proliferation of the attached cells. Our fluorescence microscopy observations for both coatings at higher magnifications revealed that the cells are well extended and exhibit an elongated morphology, similar to those on the reference sample (culture dish). The nuclei are clearly shaped, but the cell membranes form a dendritic structure. After 120h of incubation the cells on both coatings (with and without albumin) exhibited cytoplasmic links, as shown in Fig.20. After this time, the cells were well attached on the surface of the electrodeposited Ca-P coating with extending cytoplasmic process [54,105,106].

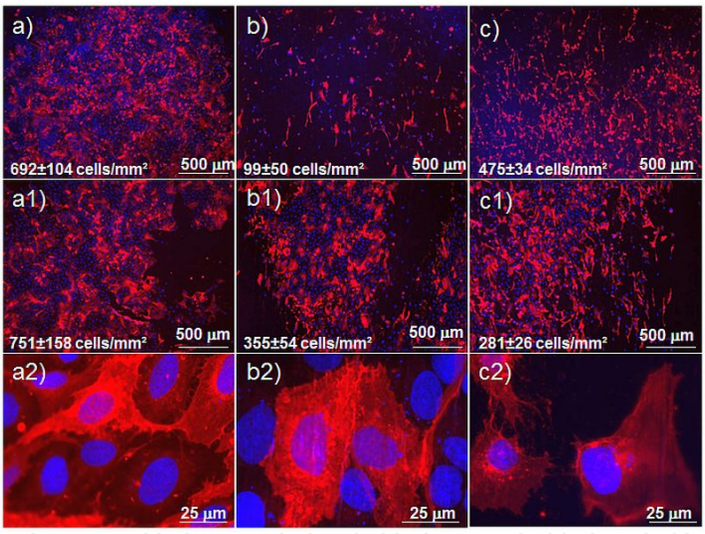

Figure 21. Fluorescence microscopy images of U2OS cells cultivated for 72 (a, b, c) and 120 h (a1, b1, c1, a2, b2, c2) on the electrodeposited Ca-P coatings on Ti without and with BSA proteins. Cell density was calculated by averaging 6 images taken randomly from the same surface. a) reference sample, culture dish; b) Ti/Ca-P: -1.5 V vs. OCP after sterilization in autoclave; c) Ti/Ca-P: -1.5 V vs. OCP after sterilization in autoclave + BSA proteins

Similar relations was observed for Ca-P coatings deposited on chemically pre-treated Ti surfaces via soaking in Hanks' solution at 37°C for 7 days. After 48 h of cell culture, cell morphology suggests good adhesion to the substrate, Fig.22. to the substrate, Fig.22., and also we can observed growth of U2OS cells on the Ca-P after 44 h of incubation was observed an increase of U2OS cells on the Ca-P coatings in relation to oxidized and unmodified Ti, see Fig.23.

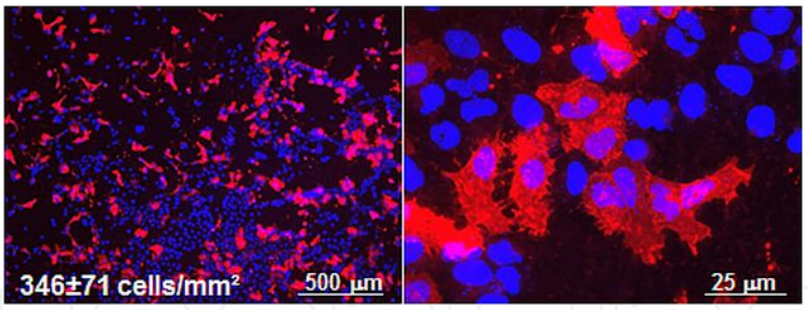

Figure 22. Fluorescence microscopy images of U2OS cells cultivated for 48 h on the Ca-P coatings deposited on TiO_2 nanotubes.

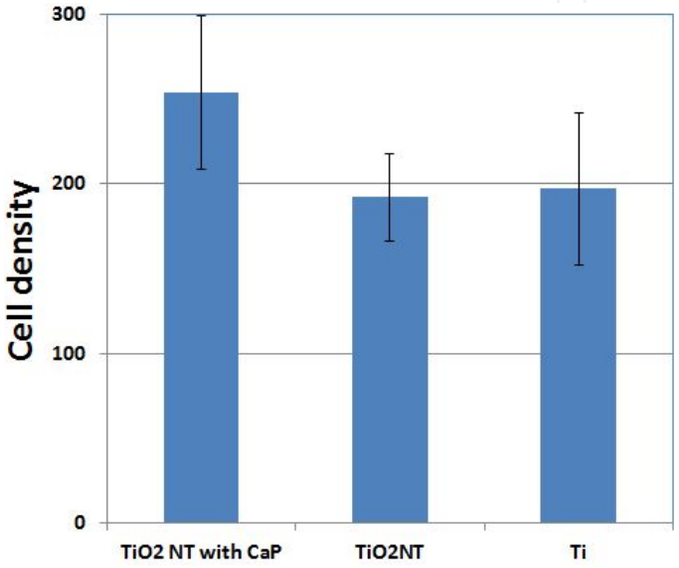

Figure 23. Cell density of the U2OS cells cultivated for 44 h on the: Ca-P coating deposited on TiO_2 nanotubes, TiO_2 nanotubes (20 V) and pure Ti (as-received state).

The ALP activity of the U2OS cells cultured on the various specimens is shown in Fig. 24 (Ca-P coatings, TiO_2 nanotubes and pure Ti). ALP test is widely used for the early stage of cell differentiation. ALP enzyme produced by osteoblasts stimulates their activity, which is responsible for the mineralization of bone tissue. After 6 days of cell culture (point 0 h), an increase of ALP activity for cells cultured on pure and modified Ti was observed. After 24 and 48 h the ALP activity is strongly associated with the cell adhesion and proliferation speed, and thus may explain the differences between cultured samples. The highest concentration of the ALP enzyme was observed for TiO_2 nanotubes. The specific morphology of the TiO_2 nanotubes probably increases the potential of differentiating cells toward osteogenesis process (the formation of new bone material by cells called osteoblasts), as also observed by other authors [70]. The accelerated growth of osteoblast cells observed on vertically aligned nanotubes and Ca-P coatings surfaces may be of importance for biomedical applications, as it could accelerate cell proliferation of other cells line. It was demonstrated that the adhesion/propagation of the osteoblasts cells is significantly improved by the morphology, chemical composition and properties of the investigated surfaces (see Fig. 21, 22) [2,107,108].

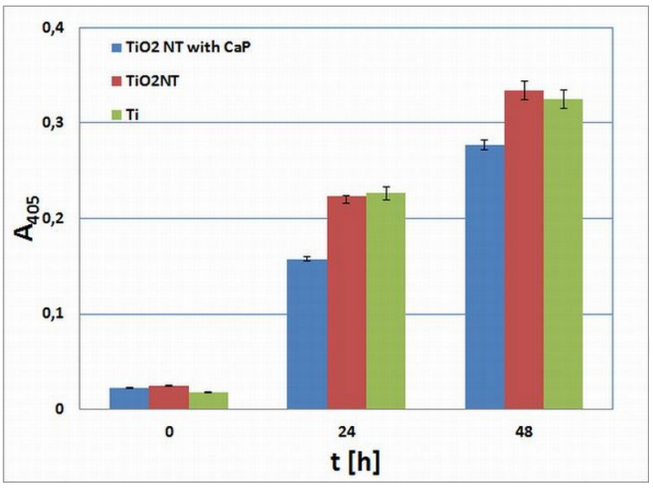

Figure 24. ALP activity of U2OS osteoblasts cells cultured on TiO_2 nanotubes, Ca-P and pure Ti.

3. Modification of Ca-P coating with silver nanoparticles: biocompatibility and antibacterial properties.

The adherence of bacteria to the biomaterial causes serious surgical complications, and poses a threat to patients with long-term implants [44,109]. Although, current methods of sterilization exist, yet in the case of the early onset of corrosion of the implant, problems with bacterial habitats still do arise. A promising method to tackle this issue is the fabrication of materials that retain biocompatibility and prevent infections. Current strategies aimed at minimizing the incidence of biomaterials associated infection involve the addition of antibacterial agents (e.g., antibiotics, specific polymers, toxic metal ions) onto the surface of implantable devices [110-113]. The primary advantage of these antibacterial coatings is the release of the bactericidal agent at the site of implantation, minimizing the risk of reaching concentrations that can cause harmful side reactions to other parts of the body.

SEM image of TiO_2 nanotube layer (top-view, before treatment) formed at V_{max} = 20 V and loaded with 0.01 mg/cm^2 of silver is shown in Figure 24. The sputter-deposited Ag formed spherical nanoparticles that are located on the top edges of the nanotubes and on their inner and outer side walls. It can be seen that the silver particles are distributed homogenously in the TiO_2 nanotube layer. Moreover, Fig. 25 shows the Ag-loaded TiO_2 nanotubes surface after soaking in Hanks' solution at 37^{o}C for 6 and 24 h. One can see an early stage of Ca-P layer formation on the top of the nanotubes after 6h immersion in Hanks' solution. Nevertheless, the Ag nanoparticles are still present at the nanotubes' edges. After immersion for 24 h, the layer become denser and better integrated with nanoporous substrate. Our previous experiments clearly indicated that Hanks' solution penetrates the interior of the TiO_2 nanotubes and the spaces between them [22], see Fig.14. The deposition of the calcium phosphate coating on the surface of the nanotubes leads to the formation of a specific composite-like layer. The vertically aligned TiO_2 nanotubes on Ti substrate act as an intermediate layer providing both the apatite-Ti binding and a mechanical stability of the composite. Also, incorporation of silver nanoparticles into apatite increases the strength and toughness of the composite as well as provides antibacterial properties [45] Thus, the composite layer investigated in this study, nano-Ag/Ca-P coating/TiO_2 nanotubes, seems to be promising for advanced biomedical applications [114].

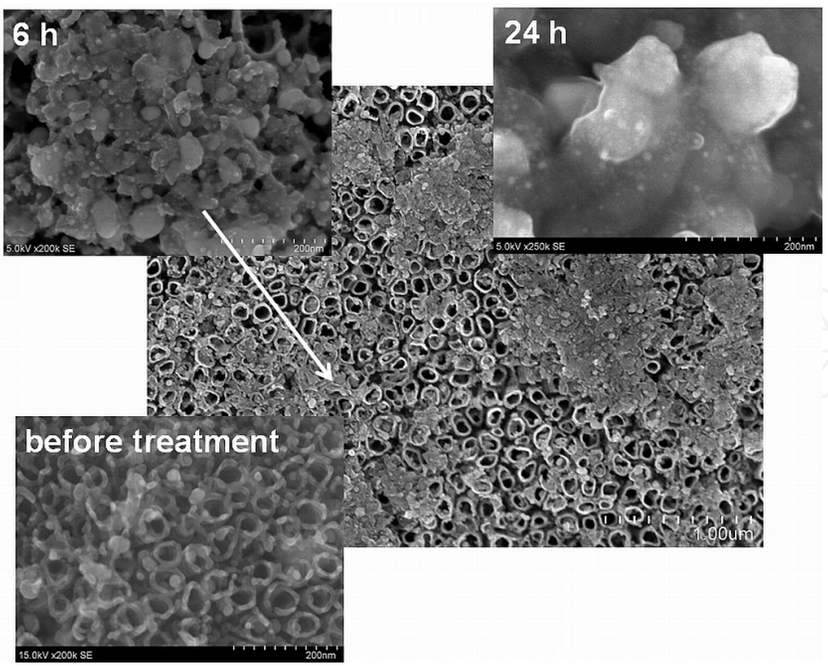

Figure 25. SEM image of typical TiO_2 nanotube layer (before treatment) formed at V_{max} = 20 V and loaded with 0.01 mg Ag/cm² and SEM images of TiO_2 NT with the same amount of Ag after immersion in Hanks' solution for 6 h and 24 h.

The enrichment of the coating with Ca and P in the present case confirmed the EDS results for the calcium phosphate coatings formed on Ag/TiO_2 nanotubes layer. The average concentrations of Ca and P increase with time of exposure to Hanks' solution. The atomic concentration ratio Ca/P for soaked samples is close to 0.73 for 6 h immersion and reaches 1.54 after 24 h, Fig.26. These results suggest that the calcium phosphate layer formed during immersion procedure tends to incorporate more Ca with time. EDS analysis revealed that the silver content in the composite layer decrease with time of immersion in Hanks' solution from ~3.5 to about 1.7 at.%. Such result could be expected, as longer exposition time of samples in simulated physiological solution leads to a partial coverage of silver nanoparticles with a layer of calcium phosphate [114].

Existing literature data show that the antibacterial action of silver is not fully understood, yet [109,115,116]. Some authors argued that the antibacterial action of Ag nanoparticles depends on the availability of silver ions [114]. Silver cations Ag^+ can bind to bacterial cell wall membrane (slightly negative) and damage it thus altering its functionality. However, other studies have shown that the cytotoxicity of Ag nanoparticles is primarily the result of the oxidative stress and is independent of the toxicity of silver ions [116]. Silver forms insoluble AgCl in Cl^- containing solution. Thus any contact with simulated body fluids would therefore prevent a release of Ag^+ from the metal phase. Nevertheless, the release of Ag^+ from Ag nanoparticles in water may provide an insight into the stability of the nanoparticles. In our study the release kinetics of Ag^+ was confirmed by ICP-MS (inductively coupled plasma mass spectrometry) measurements [114].

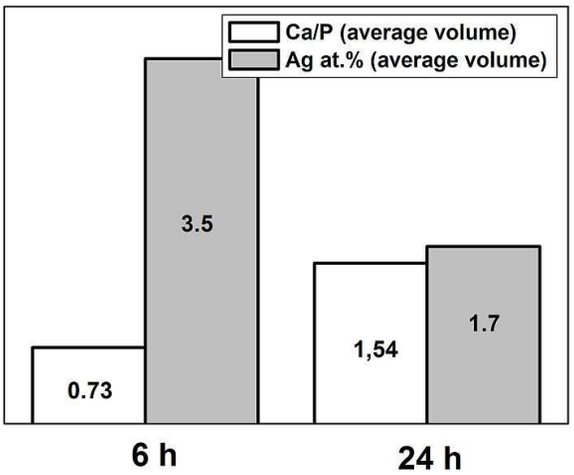

Figure 26. Results of EDS analysis Ca/P atomic ratio and silver concentration (average volume) of calcium phosphate coatings deposited on TiO_2 nanotubes loaded with 0.01 mg/cm^2 of Ag after various immersion times in Hanks' solution: 6 h, 24 h.

Fig. 27 shows the amount of silver ions released in deionized water and 0.9% NaCl solution in function of time. Silver was obviously released faster in NaCl environment than in water solution. After 3 days of incubation the release of the silver ions proceeds relatively slower in water and is stabilized below 170 μg/L. Process occurs much faster in NaCl solution, as a plateau indicating a stabilization of the release of silver ions which was not observed like for water environment. Phenomenon of rapid release of silver ions in NaCl solution may be due to the formation of AgCl during the experiment. After 7 days, less than 550 μg/L of Ag^+ were found in 0.9% NaCl solution, indicating that leaching of Ag^+ from the nanoparticles is still relatively low. Vik et al. [47] pointed out that the maximum silver concentration released in vitro should be no more than 10 mg/L. Silver becomes toxic to human cells at higher amount. Over this experiment, the silver released from Ag/TiO_2 nanotubes/Ti sample is less than the maximum cytotoxic concentration. Thus, our Ag loaded TiO_2 nanotube composite layer on Ti proved to be a promising implant material [114].

Recent studies evidenced that silver nanoparticles are more active and reactive than the bulk metallic counterpart, first of all because of their larger specific surface area [115,117]. Morones et al. [118] reported that silver particles with a preferential diameter of about 1–10 nm had direct interactions with bacteria, while larger particles did not. In view of this, the Ag/TiO_2 NT composite layer developed here with 0.01 mg/cm^2 of Ag are expected to have a great potential for biomedical applications. The well dispersed Ag nanoparticles homogeneously distributed over the TiO_2 nanotube layer are very likely to maintain a steady antibacterial effect, as long as Ag nanoparticles remain their metallic state [114].

The antibacterial activity of the Ag/TiO_2 nanotube composite layers was examined by bacterial counting method using *Staphylococcus epidermidis* (*S. epidermidis*, ATCC 12228), Fig.28. *S. epidermidis* is the most frequently isolated coagulase-negative staphylococci from implant-associated infections and have been found to be more antibiotic resistant than *S. aureus* [119]. The obtained results revealed that the deposition of Ag nanoparticles

significantly reduced the *S. epidermidis* cell adhesion and biofilm formation on modified surface. Interestingly, the TiO_2 nanotube layer (pore diameter ~75 nm) also exhibits some antibacterial properties, as reported previously [120,121]. For Ag loaded surface the amount of bacterial cell per surface area unit is about nine times lower than for pure Ti and for TiO_2 nanotubes without Ag the amount of bacterial cells is about 3 times lower comparing to pure Ti. Thus, the Ag/TiO_2 nanotube composite layers may be promising for combating post-operative infection for applications in hard tissue replacement procedures.

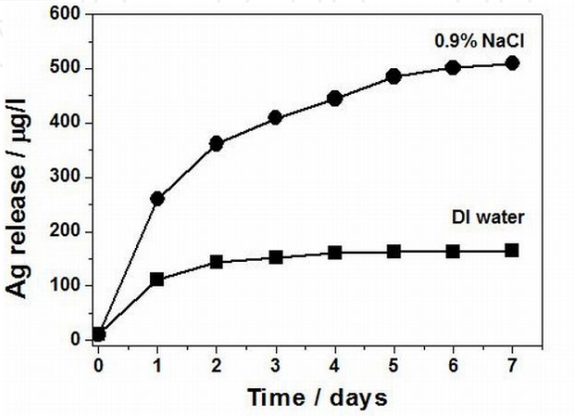

Figure 27. Amount of silver released from TiO_2 nanotubes loaded with 0.01 mg/cm² of Ag.

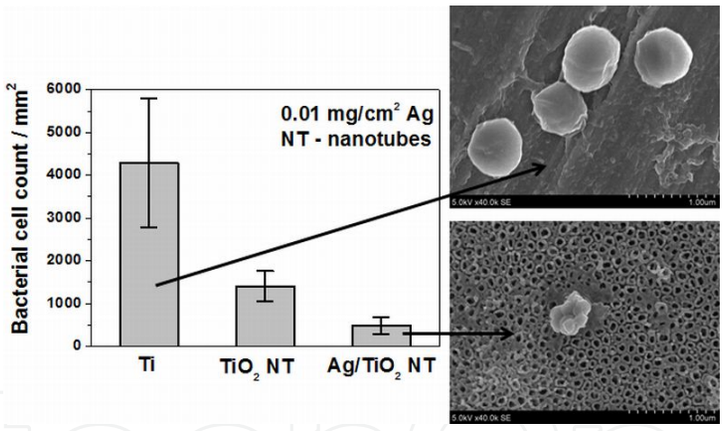

Figure 28. *S. epidermidis* cell adhesion on Ti, TiO_2 nanotubes and Ag loaded TiO_2 nanotubes.

It is noteworthy that this type of composite material has attracted the attention of material scientists and biochemists only recently. It turns out that, depending on the surface properties of the titanium substrate, the deposited biomimetic apatite layer can vary in both surface chemistry and crystallinity [122]. These subtle differences in the local microenvironment can result in significant differences in cell behavior [122].

4. Summary and conclusions

Our surface analytical and physico-chemical investigations confirmed that, the chemical treatment of a Ti surface, in both an alkaline (NaOH) and an acidic (H_2O_2 + H_3PO_4) solution, resulted in significant changes in topography/morphology, with a characteristic feature

exhibiting the presence of micro- and nano-porosities. The chemical composition of the treated surfaces did not differ significantly – Ti-oxides (mostly TiO_2) were formed at the surface as a result of both treatments. However, the new Ti(H_2O_2 + H_3PO_4) treatment led to the incorporation of some phosphates into the oxide film, which may enhance biocompatibility.

Titanium oxide nanotubes were grown on Ti in fluoride containing electrolytes with an optimum concentration of 0.86 wt.% NH_4F at a constant voltage from 10 V up to 25 V. Self-organized porous structures (nanotubes) with diameters from about ~40 up to ~110 nm and a length of ~800 μm were formed. Annealing at 600°C resulted in crystallization of the nanotube material into anatase and - what is important - in a mechanical stabilization of the nanoporous layer on a Ti substrate.

The present investigations confirm that calcium phosphate coatings of porous apatite-like structure and a specific morphology can be grown on pure titanium by electrodeposition at -1.5 V vs. OCP from the Hanks' solution. A porous Ca-P layer with a pore size gradient is formed with a compact thin overlayer. Our investigations suggest also that calcium phosphate coatings of apatite-like structure (probably B-type) and a developed morphology can be uniformly grown on a chemically/electrochemically pre-treated titanium surface already covered with a highly porous oxide layer by immersion of samples in Hanks' solution [123]. Such porous oxide layers significantly stimulate the formation of calcium phosphate phases in physiological body solution, an in vitro environment: from thermodynamically unstable phases ACP [124], which transform to crystalline calcium orthophosphates, mainly to carbonated apatites, which are of a great biological relevance [125]. Our EDS and XPS results suggest that different phosphates may be formed at the surface and in the bulk of the Ca-P coatings. The nucleation of calcium phosphate crystals on porous TiO_2 could provide better adhesion of the coating to the substrate possibly due to the interlocking of the Ca–P crystals within the pores [126,127].

Our results of XPS and FTIR investigations show that bovine serum albumin (BSA) adsorbed readily on a calcium phosphate coating prepared by chemical or electrochemical methods. The presence of adsorbed protein on the Ca–P surface enhances cell attachment and proliferation, which is favorable for achieving better biocompatibility. Thus, one may anticipate that a Ca–P coating on a porous oxide layer may promote early bone apposition and implant fixation by enhancing the chemical binding between new bone and the surface of implant materials. In the case of Ca–P coatings, surface chemistry is probably the dominant factor in the protein adsorption process and living cells adhesion.

A serious problem common to all biomaterials, namely the risk of infection, can be alleviated by incorporating Ag nanoparticles into the biomaterial surface. Our results have shown that Ag nanoparticles can be incorporated in a versatile manner, suitable for fabrication of new types of bactericidal materials and efficient in reducing the number of bacteria present at the surface. To this end silver was sputtered homogenously onto the TiO_2 nanotubes layer. The silver nanoparticles deposited guaranteed a sustained release in

deionized water and 0.9% NaCl solution at a level below a possible toxicity. Further improvement of bio-functionality of the composite layers was obtained by soaking in Hanks' solution. The present results suggest that the Ag/Ca-P/TiO_2 nanotubes composite layers may impart antibacterial property, which makes them promising to be applied in hard tissue replacement against postoperative infections.

Author details

Marcin Pisarek[1*], Agata Roguska[1,2], Lionel Marcon[3] and Mariusz Andrzejczuk[2]
[1]*Institute of Physical Chemistry, Polish Academy of Sciences, Kasprzaka, Warsaw, Poland*
[2]*Faculty of Materials Science and Engineering, Warsaw University of Technology, Woloska, Warsaw, Poland*
[3]*Interdisciplinary Research Institute, USR CNRS 3078 Parc de la Haute Borne, Villeneuve d'Ascq, France*

Acknowledgement

We are most grateful to dr Anna Belcarz from Department of Biochemistry and Biotechnology at Medical University of Lublin (Poland) and dr Maciej Spychalski from Faculty of Materials Science and Engineering at Warsaw University of Technology (Poland) for helpful discussions and to all the co-authors who contributed their knowledge and experience to the joint papers quoted in this chapter. This work was financially supported by the Polish Ministry of Science and Higher Education (Grant no. N N507 355035, IP2010 035070), the National Science Center (decision No. DEC-2011/01/B/ST5/06257) and by the Institute of Physical Chemistry PAS (Warsaw, Poland) and Interdisciplinary Research Institute (Lille, France). Surface characterizations (AES, XPS) were performed using a Microlab 350 located at the Physical Chemistry of Materials Center of the Institute of Physical Chemistry, PAS and of the Faculty of Materials Science and Engineering, WUT.

Abbreviations

HR-SEM (High Resolution – Scanning Electron Microscopy), AFM (Atomic Force Microscopy), AES (Auger Electron Spectroscopy), XPS (X-ray Photoelectron Spectroscopy), FTIR (Fourier Transform Infrared Spectroscopy), FIB (Focused Ion Beam), TEM (Transmission Electron Microscopy), BSA (Bovine Serum Albumin), Ca-P (calcium phosphate coating), SERS (Surface Enhanced Raman Spectroscopy), REF (reference substrate), R_a (average roughness), R_q (root-mean-square deviation), R_z (roughness depth), R_{max} (maximum roughness depth), SEM (Scanning Electron Microscopy), STEM (Scanning Transmission Electron Microscopy), EDS (Energy Dispersive Spectroscopy), ICP-MS (Inductively Coupled Plasma Mass Spectrometry), ACP (Amorphous Calcium Phosphate),

* Corresponding Author

DCP (Dicalcium Phosphate), OCP (Octacalcium Phosphate), ALP (Alkaline Phosphatase Test), U2OS (human osteosarcoma cell line)

5. References

[1] Diebold U. (2003) The surface science of titanium dioxide. Surf. sci. r 48:53-229.
[2] Oh S, Daraio C, Chen LH, Pisanic TR, Finones RR, Jin S. (2006) Significantly accelerated osteoblast cell growth on aligned TiO_2 nanotubes. J biomed. mater. res a. 78:97–103.
[3] Park J, Bauer S, von der Mark K, Schmuki P (2007) Nanosize and Vitality: TiO_2 nanotube diameter directs cell fate. Nano lett., 7(6):1686-1691
[4] Roguska A, Kudelski A, Pisarek M, Lewandowska M, Dolata M, Janik-Czachor M (2009) Raman investigations of TiO_2 nanotube substrates covered with thin Ag or Cu deposits. J. raman spectrosc. 40(11):1652-1656.
[5] Roguska A, Kudelski A, Pisarek M, Opara M, Janik-Czachor M (2011) Raman investigations of SERS activity of Ag nanoclusters on a TiO_2-nanotubes/Ti substrate. Vibr. spectr. 55:38–43.
[6] Roguska A, Kudelski A, Pisarek M, Opara M, Janik-Czachor M (2011) Surface-enhanced Raman scattering (SERS) activity of Ag, Au and Cu nanoclusters on TiO_2-nanotubes/Ti substrate. Appl. surf. sci. 257:8182-8189.
[7] Liu X, Chu PK, Ding Ch (2004) Surface modification of titanium, titanium alloys, and related materials for biomedical applications. Mater. sci. eng. r. 47:49-121.
[8] Liu X, Chu PK, Ding Ch (2010) Surface nano-functionalization of biomaterials. Mater. sci. eng. r. 70:275–302.
[9] Pisarek M, Lewandowska M, Roguska A, Kurzydłowski KJ, Janik-Czachor M (2007) SEM, Scanning Auger and XPS characterization of chemically pretreated Ti surfaces intended for biomedical applications. Mater. chem. phys. 104:93-97.
[10] Chen Y, Lee Chi-Y, Yeng M-Y, Chin H.T (2003) Preparing titanium oxide with various morphologies. Mater. chem. phys. 81:39-43.
[11] Wang XX, Hayakawa S, Tsuru K, Osaka A (2002) Bioactive titania gel layers formed by chemical treatment of Ti substrate with a H_2O_2/HCl solution. Biomaterials. 23:1353-1357.
[12] Kokubo T, Kim H-M, Miyaji F, Takadama H, Miyazaki T (1999) Ceramic–metal and ceramic–polymer composites prepared by a biomimetic process. Composites a. 30:405–409.
[13] Kokubo T (1998) Apatite formation on surfaces of ceramics, metals and polymers in body environment. Acta Mater. 46(7):2519–2527.
[14] Pisarek M, Roguska A, Andrzejczuk M, Marcon L, Szunerits S, Lewandowska M, Janik-Czachor M (2011) Effect of two-step functionalization of Ti by chemical processes on protein adsorption. Appl. surf. sci. 257:8196-8204.

Pisarek M, Roguska A, Marcon L, Andrzejczuk M (2012) Biomimetic Ca-P coatings obtained by chemical/electrochemical methods from Hanks' solution on a Ti surface. Eng. biomaterials. Accepted for publication.

[15] Nishiguchi S, Kato H, Fujita H, Ok M, Kim HM, Kokubo T, Nakamura T (2001) Titanium metals form direct bonding to bone after alkali and heat treatments. Biomaterials. 22:2525–2533.

[16] Takadama H, Kim H.-M, Kokubo T, Nakamura T (2001) XPS study of the process of apatite formation on bioactive Ti-6Al-4V alloy in simulated body fluid. Sci. technol. adv. mater. 2:389-396.

[17] Wei M, Kim HM, Kokubo T, Evans JH (2002) Optimizing the bioactivity of alkali treated titanium alloy. Mater. sci. eng. C. 20:125–134.

[18] Liang F, Zhou L, Wang K (2003) Apatite formation on porous titanium by alkali and heat treatment. Surf. coat. technol. 165:133–139.

[19] Park Ji-H, Lee Y.-K, Kim K.-M, Kim K.-N (2005) Bioactive calcium phosphate prepared on H_2O_2-treated titanium substrate by electrodeposition. Surf. coat. technol. 195:252-257.

[20] Zhao J, Wang X, Chen R, Li L (2005) Fabrication of titanium oxide nanotube arrays by anodic oxidation. Solid state commun. 134:705-710.

[21] Macak JM, Tsuchiya H, Ghicov A, Yasuda K, Hahn R, Bauer S, Schmuki P (2007) TiO_2 nanotubes: Self-organized electrochemical formation, properties and applications. Curr. opinion solid state mater. sci. 11:3-18.

[22] Roguska A, Pisarek M, Andrzejczuk M, Dolata M, Lewandowska M, Janik-Czachor M (2011) Characterization of a calcium phosphate -TiO_2 nanotube composite layer for biomedical applications. Mater. sci. eng c. 31:906-914.

[23] Wang H, Eliaz N, Hobbs LW (2011) The nanostructure of an electrochemically hydroxyapatite coating. Mater. lett. 65:2455-2457.

[24] Park Ji-H, Lee D-Y, Oh K-T, Lee Y-K, Kim K-M, Kim K-N (2006) Bioactivity of calcium phosphate coatings prepared by electrodeposition in a modified simulated body fluid. Mater. lett. 60:2573-2577.

[25] de Bruijn JD, van Blitterswijk CA (1998) New developments in implant coatings: biomimetics and tissue engineering. In: Walenkamp G, editor. Biomaterials in Surgery. Stuttgart, Germany: Georg Thieme Verlag; 1998. p 77–82.

[26] Royer P, Rey Ch (1991) Calcium phosphate coatings for orthopaedic prosthesis. Surf. coat. technol. 45(1-3): 171-177.

[27] Wang H, Eliaz N, Xiang Z, Hsu HP, Spector M, Hobbs LW (2006) Early bone apposition in vivo on plasma-spryed and electrochemically deposited hydroxyapatite on titanium alloy. Biomaterials. 27:4192-4203.

[28] Hanawa T, Ota M (1991) Calcium phosphate naturally formed on titanium in electrolyte solution. Biomaterials. 12(8): 767-774.

[29] Bosetti M, Masse A, Tobin E, Cannas M (2002) Silver coated material for external fixation devices; in vitro biocompatibility and genotoxicity. Biomaterials. 23:887–892.

[30] Jonasova L, Muller FA, Helebrant A, Strand J, Greil P (2004) Biomimetic apatite formation on chemically treated titanium. Biomaterials. 25:1187-1194.

[31] Wang J, Layrolle P, Stigter M, de Groot K (2004) Biomimetic and electrolytic calcium phosphate coatings on titanium alloy: physicochemical characteristics and cell attachment. Biomaterials 25:583-592.

[32] Lewandowska M, Roguska A, Pisarek M, Polak B, Janik-Czachor M, Kurzydłowski KJ (2007) Morphology and chemical characterization of Ti surfaces for biomedical applications. Biomol. Eng. 24:438-442.

[33] Kasemo B (1983) Biocompatibility of titanium implants: surface science aspects. J. prosthetic dentistry. 49:832-837.

[34] Lee B.-H, Kim YD, Lee KH (2003) XPS study of bioactive graded layer in Ti-In-Nb-Ta alloy prepared by alkali and heat treatments. Biomaterials. 24:2257-2266.

[35] Vallet-Regi M, Gonzalez-Callet JM (2004) Calcium phosphates as substitution of bone tissues. Prog. solid state chem. 32:1-31.

[36] Tsuchiya H, Macak JM, Taveira L, Balaur E, Ghicov A, Sirotna K, Schmuki P (2005) Self-organized TiO_2 nanotubes prepared in ammonium fluoride containing acetic acid electrolytes. Electrochem. commun. 7:576–580.

[37] Kodama A, Bauer S, Komatsu A, Asoh H, Ono S, Schmuki P (2009) Bioactivation of titanium surfaces using coatings of TiO_2 nanotubes rapidly pre-loaded with synthetic hydroxyapatite. Acta Biomater. 5:2322–2330.

[38] Oh S, Finones RR, Daraio Ch, Chen LH, Jin S (2005) Growth of nano-scale hydroxyapatite using chemically treated titanium oxide nanotubes. Biomaterials. 26:4938–4943.

[39] Raja KS, Misra M, Paramguru K (2005) Deposition of calcium phosphate coating on nanotubular anodized titanium. Mater. lett. 59:2137–2141.

[40] Kunze J, Muller L, Macak JM, Greil P, Schmuki P, Muller FA (2008) Time-dependent growth of biomimetic apatite on anodic TiO_2 nanotubes. Electrochim. acta. 53:6995–7003.

[41] Kar A, Raja KS, Misra M (2006) Electrodeposition of hydroxyapatite onto nanotubular TiO_2 for implant applications. Surf. coat. technol. 201:3723-3731.

[42] Wang Y-q, Tao J, Wang L, He P-t, Wang T (2008) HA coating on titanium with nanotubular TiO2 intermediate layer via electrodeposition. Trans. nonferrous met. soc. china. 18:631-635.

[43] Gristina AG, Costerton JW (1985) Bacterial adhesion to biomaterials and tissue. J. Bone Joint Surgery 67A:264-273n

[44] Gristina AG (1994) Implant failure and the immuno-incomponent fibro-inflammatory zone. Clinical orthopaedics related research. 298:106-118.

[45] Sygnatowicz M, Keyshar K, Tiwari A (2010) Antimicrobial properties of silver-doped hydroxyapatite nano-powders and thin films. JOM. 62(7):65-70.

[46] Rai M, Yadav A, Gade A (2009) Silver nanoparticles as a new generation of antimicrobials. Biotechnol. adv. 27:76-83.

[47] Vik H, Andersen KJ, Julshamn K, Todnem K (1985) Neuropathy caused by silver adsorption from arthroplasty cement. Lancet. 1:872.
[48] Fischer-Crips AC (2002) Nanoindentation. Sprinter-Verlag, New York.
[49] Dorozhkin SV, Schmitt M, Bouler JM, Daculsi G (2000) Chemical transformation of some biologically relevant calcium phosphates in aqueous media during steam sterilization. J. mater. sci. mater. med. 11:779-786.
[50] Morejon-Alonso L, Garcia Carrodeguas R, Delgado Garcia-Menocal JA, Alonso Perez JA, Martinez Manent S (2007) Effect of sterilization on the properties CDHA-OCP-β-TCP biomaterial. Mater. res. 10(1):15-20.
[51] McCafferty E, Wightman JP (1999) An X-ray photoelectron spectroscopy sputter profile study of the native air-formed oxide film on titanium. Appl. surf. sci. 143:92-100.
[52] Garbacz H, Pisarek M, Kurzydłowski KJ (2007) Corrosion resistance of nanostructured titanium. Biomole. eng. 24:559-563.
[53] Feng B, Weng J, Yang BC, Qu SX, Zhang XD (2003) Characterization of surface oxide films on titanium and adhesion of osteoblast. Biomaterials. 24:4663-4670
[54] Zhu X, Chen J, Scheideler L, Reichl R, Geis-Gerstorfer J (2004) Effects of topography and composition of titanium surface oxides on osteoblast responses. Biomaterials. 25:4087–4103.
[55] Yang B, Uchida M, Kim HM, Zhang X, Kokubo T (2004) Preparation of bioactive titanium metal via anodic oxidation treatment. Biomaterials. 25:1003–1010.
[56] Kuphasuk Ch, Oshida Y, Andres CJ, Hovijitra ST, Barco MT, Brown DT (2001) Electrochemical corrosion of Ti and titanium based alloys. J. prosthetic dentistry. 85(2):195-202
[57] Schenk R. (2001) The corrosoin properties of titanium and titanium alloys. chapter 6, pp.145-170 in "Titanium in Medicine" Eds. Brunette DM, Tengvall P, Textor M Thomsen P. Springer-Verlag.
[58] Roguska A, Hiromoto S, Yamamoto A, Woźniak MJ, Pisarek M, Lewandowska M (2011) Collagen immobilization on 316L stainless steel surface with cathodic deposition of calcium phosphate. Appl. surf. sci. 257:5037-5045.
[59] Macak JM, Hildebrand H, Marten-Jahns U, Schmuki P (2008) Mechanistic aspects and growth of large diameter self-organized TiO_2 nanotubes. J. electroanal. chem. 621:254-266.
[60] Petukhov DI, Eliseev AA, Kolesnik IV, Napolskii KS, Lukashin AV, Tretyakov YD, Griegoriev SV, Gregorieva NA, Eckerlebe H (2008) Microporous mesoporous mater. 114:440-447.
[61] Wang M, Liu Y, Yang H (2012) A unified thermodynamic theory for the formation of anodized metal oxide structures. Electrochem. acta. 62:424-432.
[62] Peltonen J, Jarn M, Areva S, Linden M, Rosenholm JB (2004) Topographical parameters for specifying a three-dimensional surface. Langmuir. 20:9428–9431.

[63] Jaroenworaluck A, Regonini D, Bowen CR, Stevens R (2010) A microscopy study of the effect of heat treatment on the structure and properties of anodised TiO_2 nanotubes. Appl. surf. sci. 256:2672-2679.

[64] Fang D, Luo Z, Huang K, Lagoudas DC (2011) Effect of heat treatment on morphology, crystalline structure and photocatalysis properties of TiO_2 nanotubes on Ti substrate and freestanding membrane. Appl. surf. sci. 257:6451-6461.

[65] Yu J, Wang B. (2010) Effect of calcination temperature on morphology and photoelectrochemical properties of anodized titanium dioxide nanotube arrays. Appl. catal. b-environ. 94:295-302.

[66] Crawford GA, Chawla N, Das K, Bose S, Bandyopadhyay A (2007) Microstructure and deformation behavior of biocompatible TiO_2 nanotubes on titanium substrate. Acta biomater. 3:359–367.

[67] Mante FK, Baran GR, Lucas B (1999) Nanoindentation studies of titanium single crystals. Biomaterials. 20:1051-1055.

[68] Wang J, Lin Z (2009) Anodic formation of ordered TiO_2 nanotube arrays: effects of electrolyte temperature and anodization potential. J. phys. chem. c. 113:4026-4030.

[69] Qian L, Du Z-L, Yang S-Y, Jin Z-S (2005) Raman study of titania nanotube by soft chemical process. J. mol. struct. 749:103-107.

[70] Brammer KS, Oh S, Frandsen ChJ, Jin S. (2010) TiO_2 nanotubes structures for enhanced cell and biological functionality. JOM. 62(4):50.

[71] A.Kudelski, A.Roguska, M.Pisarek, M.Hołdyński, M.Janik-Czachor (2012) Surface-enhanced Raman scattering (SERS) investigations on silver nanopartcles deposited on alumina and titania nanotubes: influence of the substrate material on SERS activity of Ag nanoparticles. J. raman spectrosc. accepted for publication.

[72] Barrere F, Snel MME, van Blitterswijk CA, de Groot K, Layrolle P. Nano-scale study of the nucleation and growth of calcium phosphate coating on titanium implants. Biomaterials. 25:2901-2910.

[73] Bigi A, Boanini E, Bracci B, Facchini A, Panzavolta S, Segatti F, Sturba L (2005) Nanocrystalline hydroxyapatite coatings on titanium: a new fast biomimetic method. Biomaterials. 26:4085–4089.

[74] Peltola T, Jokinen M, Rahiala H, Pätsi M, Heikkilä J, Kangasniemi I, Yli-Urpo A (2000) Effect of aging time of sol on structure and in vitro calcium phosphate formation of sol–gel derived titania films. J. biomed. mater. res. 51:200–208.

[75] Jarn M, Areva S, Pore V, Peltonen J, Linden M (2006) Topography and surface energy dependent calcium phosphate formation on sol–gel derived TiO_2 coatings. Langmuir. 22:8206–8213.

[76] Kim YH, Cho CS, Kang IK, Kim SY, Kwon OH (2007) Mechanism study of calcium phosphate deposition on a titanium surface in simulated body fluid. Key eng. mater. 342–343:693–696.

[77] Kaciulis S, Mattogno G, Napoli A, Bemporad E, Ferrari F, Montenero A, Gnappi G (1998) Surface analysis of biocompatible coatings on titanium. J. electron. spectrosc. relat. phenom. 95:61–69.
[78] Stoch A, Brozek A, Kmita G, Stoch K, Jastrzebski W, Rakowska A (2001) Electrophoretic coating of hydroxyapatite on titanium implants. J. mol. struct. 596:191–200.
[79] Kaciulis S, Mattogno G, Pandolfi L, Cavalli M, Gnappi G, Montenero A (1999) XPS study of apatite-based coatings prepared by sol–gel technique. Appl. surf. sci. 151:1–5.
[80] Zhang Q, Leng Y (2005) Electrochemical activation of titanium for biomimetic coating of calcium phosphate. Biomaterials. 26:3853–3859.
[81] Forsgren J, Svahn F, Jarmar T, Engqvist H (2007) Formation and adhesion of biomimetic hydroxyapatite deposited on titanium substrates. Acta Biomater. 3:980–984.
[82] Serro AP, Saramago B (2003) Influence of sterilization on the mineralization of titanium implants induced by incubation in various biological model fluids. Biomaterials. 24:4749-4760.
[83] Ponsonnet L, Reybier K, Jaffrezic N, Comte V, Lagneau C, Lissac M, Martelet C (2003) Relationship between surface properties (roughness, wettability) of titanium and titanium alloys and cell behavior. Mater. sci. eng. c. 23:551–560.
[84] de Gennes PG (1985) Wetting statics and dynamics. Rev. mod. phys. 57:289–324.
[85] Paital SR, Dahotre NB (2009) Wettability and kinetics of hydroxyapatite precipitation on a laser-textured Ca–P bioceramic coating. Acta Biomater. 5:2763–2772.
[86] Paital SR, Balani K, Agarwal A, Dahotre NB (2009) Fabrication and evaluation of a pulse laser-induced Ca–P coating on a Ti alloy for bioapplication. Biomed. mater. 4:015009 (10pp).
[87] Uchida M, Kim H-M, Kokubo T, Fujibayashi S, Nakamura T (2003) Structural dependence of apatite formation on titania gels in a simulated body fluid. J. biomed. mater. res. a. 64A:164–170.
[88] Lu HB, Campbell CT, Graham DJ, Ratner BD (2000) Surface characterization of hydroxyapatite and related calcium phosphates by XPS and TOF-SIMS. Anal. chem. 72:2886–2894.
[89] Dorozhkin SV (2007) Calcium orthophosphates. J. mater. sci. 42:1061–1095.
[90] Stoch A, Jastrzebski W, Brozek A, Trybalska B, Cichocinska M, Szarawara E (1999) FTIR monitoring of the growth of carbonate containing apatite layers from simulated and natural body fluids. J. mol. struct. 511–512:287–294.
[91] Muller L, Conforto E, Caillard D, Muller FA (2007) Biomimetic apatite coatings – Carbonate substitution and preferred growth orientation. Biomol. eng. 24:462–466.
[92] Koutsopoulos S (2002) Synthesis and characterization of hydroxyapatite crystals: a review study on the analytical methods. J. biomed. mater. res. 62:600–612.
[93] Nriagu JO, Moore BP (Eds.) (1984) Phosphate Minerals. Springer, Berlin.
[94] Bender SA, Bumgardner JD, Roach MD, Bessho K, Ong JL (2000) Effect of protein on the dissolution of HA coatings. Biomaterials. 21:299–305.

[95] Cai K, Bossert J, Jandt KD (2006) Does the nanometre scale topography of titanium influence protein adsorption and cell proliferation? Colloid. surf. b-biointerfaces. 49-136-144.

[96] Cai K, Frant M, Bossert J, Hildebrand G, Liefeith K, Jandt KD (2006) Surface functionalized titanium thin films: Zeta-potential, protein adsorption and cell proliferation. Colloid. surf. b-biointerfaces. 50:1–8.

[97] Feng B, Weng J, Yang BC, Qu SX, Zhang XD (2004) Characterization of titanium surfaces with calcium and phosphate and osteoblast adhesion. Biomaterials. 25:3421–3428.

[98] Deligianni DD, Katsala N, Lada S, Sotiropoulou D, Amedee J, Missirlis YF (2001) Effect of surface roughness of the titanium alloy Ti-6Al-4V on human bone marrow cell response and on protein adsorption. Biomaterials.22:1241-1251.

[99] Ahmed MH, Keyes TE, Byrne JA, Blackledge CW, Hamilton JW (2011) Adsorption and photocatalytic degradation of human serum albumin on TiO_2 and Ag-TiO_2 films. JPPA. 222: 123-131.

[100] Twardowski J, Anzenbacher P (1994) Raman and IR spectroscopy in biology and biochemistry. Warsaw: Polish Scientific Publishers PWN Ltd.

[101] Zeng H, Chittur KK, Lacefield WR (1999) Analysis of bovine serum albumin adsorption on calcium phosphate and titanium surfaces. Biomaterials. 20:377-384.

[102] Bernards MT, Qin Ch, Jiang S (2008) MC3T3-E1 cell adhesion to hydroxyapatite with adsorbed bone sialoprotein, bone osteopontin, and bovine serum albumin. Colloid. surf. b-biointerfaces. 64:236-247.

[103] Yamaguchi M, Igarashi A, Misawa H, Tsurusaki Y (2003) Enhancement of albumin expression in bone tissues with healing rat fractures. J cell biochem. 89(2): 356-363.

[104] Ishida K, Yamaguchi M Role of albumin in osteoblastic cells: Enhancement of cell proliferation and suppression of alkaline phosphatase activity (2004) Inter. j. mol. med. 14(6): 1077-1081.

[105] Park JH, Lee Y-K, Kim K-M, Kim K-N (2005) Transformation of electrodeposited calcium phosphate coatings in simulated body fluid and in culture medium. Eng. mater. 284-286:473-476.

[106] ter Brugge PJ, Dieudonne S, Jansen JA (2002) Initial interaction of U2OS cells with noncoated and calcium phosphate coated titanium substrates. J. biomed. mater. res. a. 61: 399-407.

[107] Anselme K, Linez P, Bigerelle M, Le Maguer D, Le Maguer A, Hardouin P, Hildebrand HF, Iost A, Leroy JM (2000) The relative influence of the topography and chemistry of Ti6Al4V surfaces on osteoblastic cell behaviour. Biomaterials 21:1567-1577.

[108] von Wilmowsky C, Bauer S, Roedl S, Neukam FW, Schmuki P, Schlegel KA (2012) The diameter of anodic TiO_2 nanotubes affects bone formation and correlates with the bone morphogenetic protein-2 expression in vivo. Clinical oral impl. res. 23(3):359–366.

[109] Hanssen AD, Rand JA (1998) Evaluation and treatment of infection at the site of a total hip or knee arthroplasty. J. bone joint surg. 80A:910–922.

[110] Popat CK, Eltgroth M, La Tempa JT, Grimes AC, Desai AT (2007) Decreased Staphylococcus epidermis adhesion and increased osteoblast functionality on antibiotic-loaded titania nanotubes. Biomaterials. 228:4880–4888.

[111] Chua PH, Neoh KG, Kang ET, Wang W (2008) Surface functionalization of titanium with hyaluronic acid/chitosan polyelectrolyte multilayers and RGD for promoting osteoblast functions and inhibiting bacterial adhesion. Biomaterials. 29:1412–142.

[112] Wan YZ, Xiong GY, Liang H, Raman S, He F, Huang Y (2007) Modification of medical metals by ion implantation of copper. Appl. surf. sc.i 253:9426–9429.

[113] Monteiro DR, Gorup LF, Takamiya AS, Ruvollo-Filho AC, de Camargo ER, Barros Barbosa D (2009) The growing importance of materials that prevent microbial adhesion: Antimicrobial effect of medical devices containing silver. Int. j. antimicrob. agents. 34: 103–110.

[114] Roguska A, Pisarek M, Andrzejczuk M, Lewandowska M, Kurzydłowski KJ, Janik-Czachor M (2012) Surface characterization of Ca-P/Ag/TiO_2 nanotube composite layers on Ti intended for biomedical applications. J biomed. res. a. Accepted for publication.

[115] Chen X, Schluesener HJ (2007) Nanosilver: A nanoproduct in medical application. Toxicol. let. 176:1–12.

[116] Lok CN, Ho CM, Chen R, He QY, Yu WY, Sun H, Tam PK, Chiu J-F, Che C-M (2007) Silver nanoparticles: Partial oxidation and antibacterial activities. J. boil. Inorg. Chem. 12:527–534.

[117] Kim JS, Kuk E, Yu KN, Kim JH, Park SJ, Lee HJ, Kim SH, Park YK, Park YH, Hwang CY, Kim YK, Lee YS, Jeong DH, Cho MH (2007) Antimicrobial effects of silver nanoparticles. Nanomed. nanotechnol. biol. mned. 3:95–101.

[118] Morones JR, Elechiguerra JL, Camacho A, Holt K, Kouri JB, Ramirez JT, Yacamen MJ (2005) The bactericidal effect of silver nanoparticles. Nanotechnology. 16:2346–2353.

[119] Necula BS, Fratila-Apachitei LE, Zaat SAJ, Apachitei I, Duszczyk J (2009) In vitro antibacterial activity of porous TiO_2–Ag composite layers against methicillin-resistant Staphylococcus aureus. Acta biomater. 5:3573–3580.

[120] von Wilmowsky C, Bauer S, Lutz R, Meisel M, Neukam FW, Toyoshima T, Schmuki P, Nkenke E, Schlegel KA (2009) In vivo evaluation of anodic TiO_2 nanotubes: An experimental study in the pig. Biomed. mater. res. b appl. biomater. 89:165-171.

[121] Zhao L, Chu PK, Zhang Y, Wu Z (2009) Antibacterial coatings on titanium implants. J. Biomed. Mater. Res. B. 91B(1):470-480

[122] Adams CS, Mansfield K, Perlot RL, Shapiro IM (2001) Matrix regulation of skeletal cell apoptosis – the role of calcium and phosphate ions. J. biol. chem. 276:20316–20322.

[123] Rey C, Combes C, Drouet C, Sfihi H, Barroug A (2007) Physico-chemical properties of nanocrystalline apatites: Implications for biominerals and biomaterials. Mater. sci. eng. c. 27:198-205.

[124] Dorozhkin SV (2010) Amorphous calcium (ortho)phosphates. Acta biomater. 6:4457-4475.

[125] Suzuki O (2010) Octacalcium phosphate: Osteoconductivity and a crystal chemistry. Acta biomater. 6:3379–3387.

[126] Pittrof A, Bauer S, Schmuki P (2011) Micropatterned TiO_2 nanotube surfaces for site-selective nucleation of hydroxyapatite from simulated body fluid. Acta biomater. 7(1):424-431.

[127] Dey T, Roy P, Fabry B, Schmuki P (2011) Anodic mesoporous TiO_2 layer on Ti for enhanced formation of biomimetic hydroxyapatite. Acta biomater. 7:1873-1879.

IntechOpen